

Exciting the Domain Wall Soliton

Jose J. Blanco-Pillado^{1,2, *}, Daniel Jiménez-Aguilar^{1, †} and Jon Urrestilla^{1, ‡}

¹ *Department of Theoretical Physics,*

UPV/EHU, 48080, Bilbao, Spain

² *IKERBASQUE,*

Basque Foundation for Science,

48011, Bilbao, Spain

Abstract

Many solitonic configurations in field theory have localized bound states in their spectrum of linear perturbations. This opens up the possibility of having long lived excitations of these solitons that could affect their dynamics. We start the study of these effects in the simplest configuration of a domain wall kink solution in the $\lambda\phi^4$ theory in 1 + 1 dimensions. We show that this solution has a single bound state and numerically study its slow decay rate in flat space. We then investigate the amplitude of this excitation by simulating a cosmological phase transition that leads to the formation of these kinks in an expanding universe. We find that kinks get formed with a 20% excess of energy with respect to their lowest energy configuration. We also explore the kink solution interacting with a thermal bath and extract the amplitude of the localized excitation as a function of temperature. We note that this amplitude increases with temperature but again the extra energy in the kink never goes over the 20% level. Finally, we argue that this extra energy may have important consequences in the subsequent evolution of defects in numerical simulations.

Keywords: Cosmic strings, domain walls, monopoles, cosmological phase transitions.

* josejuan.blanco@ehu.eus

† daniel.jimenez@ehu.eus

‡ jon.urrestilla@ehu.eus

I. INTRODUCTION

Non linear field theories are present in many interesting physical situations. The presence of these non-linearities allow these theories to have, in their spectra of excitations, solitonic like configurations that could play a significant role in their dynamics. Examples of this type of solutions can be found in many areas of physics from condensed matter [1] to particle physics [2], string theory [3] or cosmology [4].

These solitonic solutions can be obtained by considering the lowest energy configurations of the fields involved with a particular boundary condition at infinity. An example of this idea can be found in theories with topological defects where the stability of the solutions is guaranteed by their topological charge. These objects have been extensively studied in the literature in the past decades. In $3 + 1$ dimensions one can find solitonic objects of different dimensionality like domain walls [5], cosmic strings [6] or monopoles [7, 8]¹.

On the other hand, solitons are not the only long lived localized structures that can exist in non-linear field theories. Many of the same models that have solitons also support lump-like field arrangements that could have extremely long lifetimes. One of the most prominent examples of this type of objects are oscillons² [9–12]. These configurations are not exact solutions of the equations of motion and present a very slow radiating process that allows the energy to leak to infinity in terms of small amplitude oscillations of the field around its vacuum.

In this paper we will show how in some field theories it is natural to expect the existence of some excited soliton solutions whose properties resemble in many cases the oscillon-like objects. In fact, we will show that the interactions between solitons and oscillons would give rise to these excited states which decay with a characteristically long time scale. These localized excitations could become relevant for the dynamics of the solitons, specially if they last for long periods of time. If this was the case, they could become important even at low energies. This would significantly modify the standard lore where at energies well below the energy scale of the soliton one expects that its internal deformations would not be excited.

Usually, one assumes that at low enough energies solitons should behave as coherent

¹ One could also consider instantons and textures as part of this family of solutions. However, we do not have much to add about these type of objects in this paper.

² Depending on the theory they are also called Quasi-breathers or Pulsions.

objects of their dimensionality, namely, walls, strings or point like objects. In this limit, one can easily write an effective theory for their low energy dynamics: the so-called thin wall approximation, where the soliton's width does not play any role. In the case of relativistic strings, this type of dynamics is described by the Nambu-Goto (NG) action [13, 14]. Lattice field theory simulations of individual strings have shown that this NG action is indeed a very good approximation for the motion of the strings. In fact, simulations show that only regions of the string evolution that reach high curvature deviate from the NG predictions [15].

However, large scale lattice field theory simulations of cosmic strings seem to imply that a string network behaves quite differently from what is predicted by the NG dynamics [16, 17]. These differences are quite substantial and affect very significantly the observational effects on strings, in particular their predictions regarding their gravitational wave signatures [17–19]. Given the significant progress in the observational bounds on gravitational wave signals, this uncertainty in the predictions from cosmic string networks is becoming a very pressing issue that needs to be resolved. One of the suggestions that has been put forward in the literature in trying to explain the different behavior of lattice field theory strings is the possibility that cosmological evolution of the network could lead to very excited strings [17]. These excitations could affect the evolution of the strings if they are present for long enough in the history of the network.

In this paper we take a step back and study the evolution of a much simpler field theory model based on a single real scalar field, the $\lambda\phi^4$ model. We will argue that this simple field theory has many of the properties that are important to understand the cosmic string scenario. The theory possesses field theory solitonic solutions that can be in an excited state. In the following sections we will show that these excited states have a very long lifetime that can affect the long term evolution of their field theory network simulations. However, in order to understand the impact of these excited modes, one should first show that they can be dynamically excited. In this paper we start this investigation by looking at the possible excitation of the solitons in this model through their cosmological formation in a lattice field theory model in $1 + 1$ dimensions.

The organization of the paper is the following. We introduce in Section (II) the exact solution for the kink soliton that we will be discussing in the rest of the paper. In Section (III) we describe the spectrum of excitations of this soliton and their phys-

ical interpretation. In Section (IV) we comment on the possible existence of breather solutions in the $\lambda\phi^4$ theory that we are studying. In Section (V) we study numerically the non-linear decay of the bound state modes in flat spacetime. In Section (VI) we investigate the solutions in an expanding universe. In Section (VII) we simulate the formation of these kinks in a phase transition in an expanding universe. We can then obtain the average level of excitation of the kinks at formation. In Section (VIII) we also explore the process of excitation when the kinks are in contact with a thermal bath and look at the dependence of the excitation with the background temperature. We conclude with a brief discussion of the possible impact of these results. In an attempt to make the paper easier to read, we have moved many of the technical discussions to the appendices.

The animations corresponding to some of the simulations described in the following sections can be found at <http://tp.lc.ehu.es/earlyuniverse/kink-simulations/>.

II. THE KINK SOLUTION IN $\lambda\phi^4$

Let us introduce the model we are interested in, the so-called $\lambda\phi^4$ model, whose action is given by

$$S_{\lambda\phi^4} = \int dx^2 \left[\frac{1}{2} \partial_\mu \phi \partial^\mu \phi - V(\phi) \right] = \int dx^2 \left[\frac{1}{2} \partial_\mu \phi \partial^\mu \phi - \frac{\lambda}{4} (\phi^2 - \eta^2)^2 \right]. \quad (1)$$

This is a 1+1 dimensional model where we are using a metric signature of (+1,-1). The potential of this model has two degenerate minima at $\phi = \pm\eta$ and the fluctuations around these minima are characterized by perturbative excitations of mass $m^2 = 2\lambda\eta^2$.

Apart from these excitations, it is also well known that this theory possesses non-perturbative states that interpolate between both vacua. For example, the so-called kink solutions interpolate between the $\phi = -\eta$ and the $\phi = +\eta$ minima as x grows. Due to translational invariance, the zero of the kink solution is a free parameter. The kink solution centered at the point x_0 is given by [20]

$$\phi_{k,x_0}(x) = \eta \tanh \left(\sqrt{\frac{\lambda}{2}} \eta (x - x_0) \right) = \eta \tanh \left(\frac{m}{2} (x - x_0) \right). \quad (2)$$

We will be mostly dealing with the kink centered at the origin ($x_0 = 0$): $\phi_k \equiv \phi_{k,x_0=0}$.

These solitonic³ solutions have an energy density which is exponentially localized around their center, and one can estimate their width to be of the order of $\delta_K \sim \sqrt{\frac{2}{\lambda}}\eta^{-1}$.

Furthermore, the total energy of these states can easily be computed to be

$$M_k = \frac{2\sqrt{2\lambda}}{3}\eta^3 . \quad (3)$$

One can also find the solutions that interpolate between these vacua but with the opposite boundary conditions at infinity, in other words, solutions with a different orientation, which are normally described as anti-kink solutions. We will refer to both kinks and anti-kinks generically as kinks, unless the distinction is relevant.

Many different aspects of kink and anti-kinks and their interactions have been extensively studied in the literature over the years using a combination of analytic as well as numerical techniques [21]. One interesting point about this model is its lack of integrability. This makes this model quite different in many respects to its integrable counterpart, the Sine-Gordon (SG) model [22].

A simple example where one can see the difference between these models is in the interaction between kink and anti-kink. In the SG model, the two solitons scatter off each other without any radiation. On the other hand, in the $\lambda\phi^4$ model, one has a complicated outcome of the collision that depends on the initial state [23–25]. Since kinks in the $\lambda\phi^4$ model radiate upon their interactions, and also since they suffer excitations, they are not strictly speaking solitons, and some authors refer to this type of non-perturbative configurations as solitary waves. We will use both these terms indistinguishably throughout the paper.

Another important case where these models are different is in the existence of breather solutions. In the SG case, one can find analytic solutions describing a bound state of kink and anti-kink oscillating around their center of mass [20]. In the $\lambda\phi^4$ model, one can show that there is no stable configuration of this form [26]. This does not mean, however, that there are not long lasting configurations of this type. In fact, one can easily create these localized oscillating states that slowly decay by emitting radiation. Furthermore, their interpretation as kink-anti-kink bound states was also given after some of the first numerical experiments performed in this model [9]. We will discuss more about these type of solutions later in the paper in relation to the kink excitations.

³ Strictly speaking these are not solitons, see below.

III. THE SPECTRUM OF EXCITATIONS AROUND THE KINK

Let us characterize the small perturbations about the static kink solutions presented earlier. We will assume the field to be separated into the kink solution plus perturbations as

$$\phi(x, t) = \phi_k(x) + \psi(x, t), \quad (4)$$

where $|\psi| \ll \eta$. The linearized equations of motion for these perturbations become

$$\ddot{\psi} - \psi'' + \lambda [3\phi_k^2(x) - \eta^2] \psi = 0, \quad (5)$$

where the dots and primes denote derivatives with respect to time and space respectively. Taking an oscillatory ansatz for the perturbations of the form $\psi(x, t) \propto e^{-i\omega t} f(x)$, the equation for the transverse profile of the perturbations has the form of a Schrödinger-like equation:

$$-f''(x) + U(x)f(x) = \omega^2 f(x), \quad (6)$$

with potential

$$U(x) = \lambda [3\phi_k^2(x) - \eta^2]. \quad (7)$$

This turns out to be a completely solvable potential (see [27]). Its spectrum is composed of two discrete modes and a continuum of scattering states [20]. The two discrete modes are

$$f_0(x) = \operatorname{sech}^2\left(\frac{mx}{2}\right) \quad \text{with} \quad \omega_0 = 0, \quad (8)$$

and

$$f_s(x) = \sinh\left(\frac{mx}{2}\right) \operatorname{sech}^2\left(\frac{mx}{2}\right) \quad \text{with} \quad \omega_s = \frac{\sqrt{3}}{2}m, \quad (9)$$

and the continuum of scattering states have a functional form given by

$$f_k(x) = e^{ikx} \left[3 \tanh^2\left(\frac{mx}{2}\right) - 1 - \frac{4k^2}{m^2} - i \frac{6k}{m} \tanh\left(\frac{mx}{2}\right) \right], \quad (10)$$

where $\omega_k^2 = k^2 + m^2$. Thus, their frequencies are in the range $m < \omega_k < \infty$. These last functions become the plane wave solutions for asymptotically large values of x . These plane waves are the ones associated with the continuum of perturbative fluctuations around the vacuum, the asymptotic particle states.

The physical interpretation of the two discrete modes is straightforward. The zero mode describes small rigid perturbations of the position of the soliton itself. One can see this by computing the change of the field distribution due to a small shift in the kink position, namely

$$\phi_k(x + \delta x) \approx \phi_k(x) + \frac{d\phi_k(x)}{dx} \delta x, \quad (11)$$

and noticing that

$$\frac{d\phi_k(x)}{dx} \delta x \propto \operatorname{sech}^2\left(\frac{mx}{2}\right) \propto f_0(x). \quad (12)$$

The other bound state modifies the width of the kink. One can also build some intuition for the spatial shape of this mode by performing a small variation of the thickness of the kink solution to get

$$\phi_k(x/(1 + \delta\Delta)) \approx \phi_k(x) - x \frac{d\phi_k(x)}{dx} \delta\Delta \approx \phi_k(x) - \frac{m\eta}{2} x \operatorname{sech}^2\left(\frac{mx}{2}\right) \delta\Delta. \quad (13)$$

Direct comparison between this last expression and the bound state $f_s(x)$ shows that they have a very similar profile, which suggests the name *shape mode*⁴ for this bound state. Throughout this paper we will refer to this state as *shape mode*, *bound state* or *internal mode*.

IV. BREATHER SOLUTIONS

As we mentioned in the introduction, this model has other type of interesting configurations with an extraordinarily long lifetime, first discovered by numerical experiments a long time ago in [9]. They describe the oscillation of the kink and anti-kink around each other and they share many of the properties of the Sine-Gordon breather exact solutions [20]. This motivated the pursue of approximate expressions for these type of time-dependent configurations as well as their numerical exploration by several groups [24]. In [22], the authors gave an approximate ansatz for these objects as a perturbative expansion in the (small) amplitude. However, it was shown in [26] that all these attempts to construct these periodic, localized solutions were flawed by the presence of a radiating tail⁵. This implied that

⁴ A collective coordinate approach can also be used to single out the translation as well as the width degrees of freedom. It is interesting to see that this approach yields a spectrum quite similar to the linear field theory calculation. (See for example [28]).

⁵ This is why many people refer to these configurations as quasi-breathers to remark their lack of true periodicity.

all these oscillating solutions had a finite lifetime, although in some cases they could stay around for a long enough time, such that they could play a significant role in the dynamics. One can think of these configurations as the 1 + 1 dimensional version of the pulson [10, 11] or the oscillon [12] that appear in many higher dimensional field theories.

Since we will later on encounter these objects in the course of our simulations, it is useful to describe them now. In the small amplitude regime, one can find solutions of the equations of motion to order $O(\tilde{\epsilon}^2)$ of the form [22]

$$\phi_B(x, t) = \eta \left(1 + \frac{2}{3} \tilde{\epsilon} \operatorname{sech}(\tilde{\epsilon}\sqrt{\lambda}\eta x) \cos(\tilde{\omega}_B\sqrt{\lambda}\eta t) + \tilde{\epsilon}^2 \operatorname{sech}(\tilde{\epsilon}\sqrt{\lambda}\eta x)^2 \left(\frac{1}{6} \cos(2\tilde{\omega}_B\sqrt{\lambda}\eta t) - \frac{1}{2} \right) \right),$$

where one must adjust the frequency of oscillation for different amplitudes and widths of the object using the relation

$$\tilde{\omega}_B = \sqrt{2 - \tilde{\epsilon}^2} \quad . \quad (14)$$

Looking at this expression, one realizes that, at the lowest order, these solutions always oscillate with frequencies lower than the mass of the perturbative excitations in the vacuum. In other words, we always have $w_B = \tilde{\omega}_B\sqrt{\lambda}\eta < m$. This means that, at the lowest order, these excitations are not able to emit radiation (see the discussion on scattering states in the previous section). However, it is clear that $O(\tilde{\epsilon}^2)$ terms or higher could decay by coupling these solutions to the scattering modes. This is why these configurations have such a slow decay rate and last for such a long time.

In the following we will show that, in a high energy background, these objects can be created together with kinks, and thus they could easily run into each other. In fact, in the course of our simulations we have seen breathers interacting with kinks and exciting the kink's shape mode in a significant way. This is easily understood by noticing that the breather like solutions have a large overlap with the shape mode. This relation can be made much more apparent by looking at a particular type of breather with amplitude $\tilde{\epsilon} = \frac{1}{\sqrt{2}}$, such that its width and fundamental frequency agree with the characteristic ones of the shape mode. In this case, at lowest order, the breather looks like

$$\phi_B(x, t) = \eta \left(1 + \frac{2}{3\sqrt{2}} \operatorname{sech}\left(\frac{mx}{2}\right) \cos\left(\frac{\sqrt{3}m}{2}t\right) + O(\tilde{\epsilon}^2) \right), \quad (15)$$

which suggests that an excited kink with a non zero amplitude of its shape mode can be understood as the combination of the kink and the breather. In other words, we notice that

$$\left[\tanh\left(\frac{m}{2}x\right) \times \phi_B(x, t) \right] - \phi_k(x) \propto f_s(x) \cos(w_s t). \quad (16)$$

This realization suggests that the localized shape mode of the kink can be thought of as a sort of breather trapped by the soliton. The connection between these types of objects has also been explored in the literature recently in [29].

V. NUMERICAL INVESTIGATIONS FOR THE SHAPE MODE

A. Preliminaries

Since we will make extensive use of numerical simulations throughout the paper, it will be convenient to reformulate our theory in terms of the following dimensionless quantities:

$$\tilde{\phi} = \frac{\phi}{\eta} \quad \tilde{x} = \sqrt{\lambda}\eta x \quad \tilde{t} = \sqrt{\lambda}\eta t \quad . \quad (17)$$

With these redefinitions, the action becomes

$$S = \eta^2 \int d^2\tilde{x} \left[\frac{1}{2} \partial_\mu \tilde{\phi} \partial^\mu \tilde{\phi} - \frac{1}{4} (\tilde{\phi}^2 - 1)^2 \right], \quad (18)$$

and the equation of motion in terms of the rescaled quantities is

$$\ddot{\tilde{\phi}} - \tilde{\phi}'' - \tilde{\phi} + \tilde{\phi}^3 = 0 \quad . \quad (19)$$

Note that in these units the mass of perturbative excitations around the vacua is $\tilde{m} = \sqrt{2}$, and, for example, the frequency of the shape mode is $\tilde{\omega}_s = \sqrt{\frac{3}{2}}$. The dimensionless period for the shape mode is then $P = 2\pi/\tilde{\omega}_s \approx 5.1302$, which will be used as a unit of time in most of the subsequent plots. In the rest of the paper we only work with dimensionless quantities unless otherwise specified, but for simplicity of the notation we will drop the tildes over them.

The solutions of these equations will describe the evolution of the physical system in any point of the two dimensional space of field theories parametrized by (η, λ) . Note that even though the parameter η^2 is absent from the dimensionless classical equations of motion, it appears as an overall coefficient in the action, and therefore it does have implications at the quantum level⁶. This will be of importance in Sections VII and VIII.

⁶ In fact, η plays the role of the inverse of a coupling constant so the weak coupling regime corresponds to the $\eta \gg 1$ limit. One can see this by looking at the ratio of the soliton and elementary excitation masses, namely $M_k/m \sim \eta^2$.

1. *Extracting the amplitude of the shape mode*

In the following we will describe several different lattice simulations that we have done to understand the level of excitation that the kink solutions can acquire. It is therefore paramount for us to be able to quantify this in a precise way. We do this by computing the amplitude of the shape mode of the kink directly from the simulation data.

We first note that the solutions to the Schrödinger-like equations for the linear perturbations described in the previous section form an orthonormal basis. Thus, the general expansion for a linear perturbation around the kink can be written in dimensionless units as

$$\delta(x, t) = \hat{A}_0 \bar{f}_0(x) + \hat{A}_s \bar{f}_s(x) \cos(w_s t) + \int dk \hat{A}_k \text{Re}[\bar{f}_k(x) e^{-i w_k t}] , \quad (20)$$

where we have denoted by $\bar{f}_i(x)$ the normalized mode functions ⁷.

However, since the model is non-linear, the interaction between different modes will make the \hat{A}_i coefficients above time-dependent:

$$\delta(x, t) = \hat{A}_0(t) \bar{f}_0(x) + \hat{A}_s(t) \bar{f}_s(x) \cos(w_s t) + \int dk \hat{A}_k(t) \text{Re}[\bar{f}_k(x) e^{-i w_k t}] \quad (22)$$

$$= A_0(t) \bar{f}_0(x) + A_s(t) \bar{f}_s(x) + f_r(x, t) , \quad (23)$$

where (in the last line) we have absorbed all the time dependency into the $A_i(t)$ and we have defined the integral carrying the information for the radiation as f_r .

To extract the values of A_i (in particular, $A_s(t)$) given a configuration $\phi(x, t)$ consisting of a kink plus excitation, we first obtain the point x_0 where the field ϕ goes through zero, and define that as the center of the kink. We then calculate the perturbations around the kink as

$$\phi_{\text{pert}}(x, t) = \phi(x, t) - \phi_{k, x_0}(x, t) \quad (24)$$

and finally project the perturbations over the shape mode by computing:

$$A_s(t) = \int_{-L/2}^{L/2} dx \phi_{\text{pert}}(x, t) \bar{f}_s(x - x_0) . \quad (25)$$

⁷ The normalized shape mode function in dimensionless units is given by

$$\bar{f}_s(x) = \frac{\sqrt{3\sqrt{2}}}{2} \sinh\left(\frac{x}{\sqrt{2}}\right) \text{sech}^2\left(\frac{x}{\sqrt{2}}\right) \quad (21)$$

This is the quantity that we will follow during the evolution of the kink in different situations and that we will compare with analytic predictions in the subsequent sections.

2. Numerical calculations in the lattice

Throughout this work we have solved the equation of motion (19) in a lattice. The details of its implementation can be found in Appendix (A), but here we would like to emphasize a few points that will become important in the rest of the paper. Since we are dealing with a $1 + 1$ dimensional lattice, we can use a large array of points in the spatial direction without too much computational cost. Moreover, we have written the code in a parallelized fashion so we can use many nodes to implement the evolution of a large volume. The combination of these two facts has allowed us to explore a considerable large volume in our simulations while still faithfully representing the dynamics of the fields.

This will become more advantageous later in the paper, since some of our simulations will be performed in an expanding background with comoving coordinates. In that situation, there is a well-known problem: the comoving size of the solitons in these expanding backgrounds shrinks with time. This means that by the end of the simulation one could have too small a number of comoving lattice points in the relevant central region of the kink. That is why the use of a large number of points, and a parallel code, are helpful to make sure that our final configurations had at least 20 points covering the important central region where the bound state has its support.

A somewhat popular way to deal with this issue is the so-called "fat string algorithms" [30], where the equations of motion are modified to change the rate of contraction of the soliton width in comoving coordinates. This allows the possibility to track down the position of the solitons without introducing more points in the lattice. However, this method affects, by construction, the physical width of the soliton in the simulation. This will clearly distort the level of excitation of the shape mode in an artificial way, hence we refrain from using such algorithms here.

It is also worth emphasizing that we use absorbing boundary conditions [31] in our simulations. As their name indicates, these boundary conditions work in such a way that they mimic the absorption of waves by the boundary. As we will see shortly, we will need to simulate the system for times much, much longer than the light-crossing time of the box.

This poses a numerical problem since we do not want to have the radiation energy bounce back from the edge of the simulation. This is a particularly important concern in this case because in one spatial dimension there will not be any dilution of the radiation. That is why we use absorbing boundary conditions, since they allow us to run the simulation for as long as we want and compare the results with the theoretical predictions. Actually, since we will be mostly dealing with frequencies coming from the radiation from the shape mode, we have tuned these boundary conditions such that they will be most effective at those frequencies (See the discussion in the Appendix A 2.).

B. Lifetime of the excitation

Our starting point is a detailed study of the shape mode excitation of the kink and its decay. In order to do that, we initialize our $(1 + 1)$ dimensional lattice field with a kink at the center of the box and we add to it a small perturbation of the form of the linear excitation described earlier as the shape bound state:

$$\phi(x, t) = \phi_k(x) + A(0) \times \bar{f}_s(x). \quad (26)$$

We are taking a small amplitude, $A(0) < 1$, and we do not give the field any initial velocity. Following the discussion on linear modes given earlier, one would think that this configuration should stay oscillating without any variation. The reason for this is that the value of its frequency is smaller than the ones that are allowed to propagate outside of the kink towards infinity. However, the full system is non-linear, so the amplitude of this bound state is expected to decrease over time by emitting radiation at a small rate.

At the lowest order, the non-linear terms will produce a radiation field with a frequency which doubles the bound state one and a quadratically suppressed amplitude. This clearly means that the lifetime of these perturbations will be much, much longer than the typical scale of the problem, i.e., the light-crossing time of the width of the soliton. Actually, it is likely to be a much longer time than the light-crossing time of the simulation box as well. This is why we use the aforementioned absorbing boundary conditions (see Appendix A 2.).

The problem of studying the decay of a small fluctuation like the one we just presented has been analyzed by Manton and Merabet [32] using analytical techniques. Their conclusion was

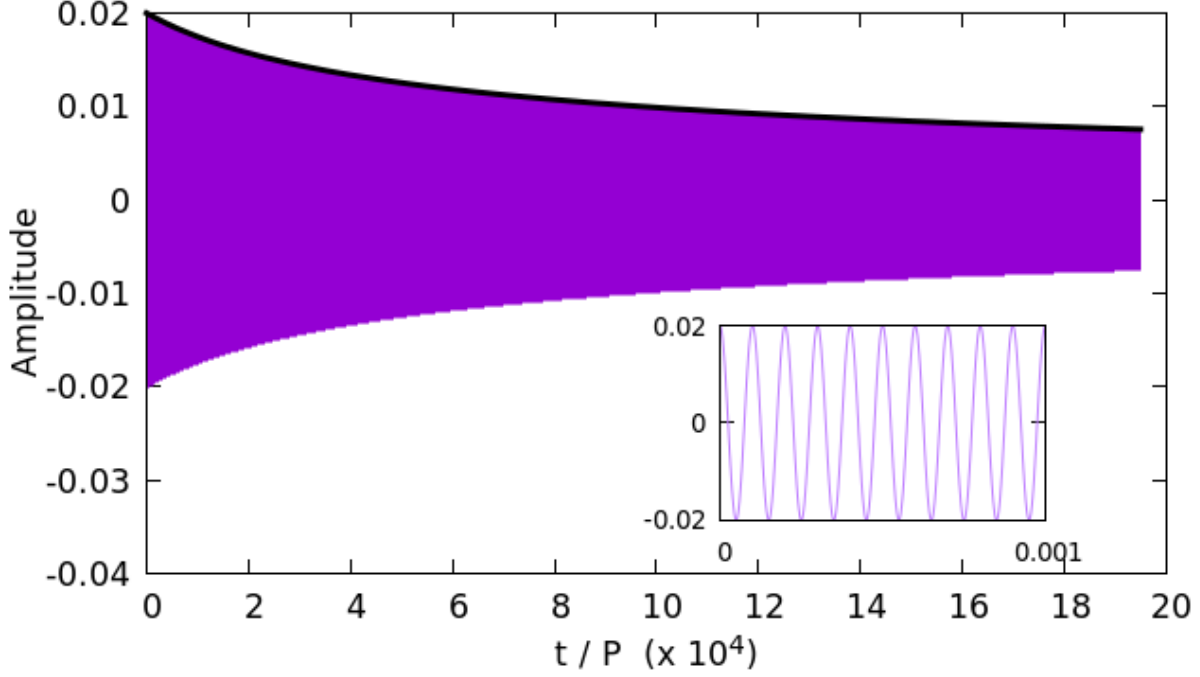


FIG. 1: Amplitude of the shape mode $A(t)$ as a function of time (displayed as number of periods or oscillations). P is the dimensionless period of the shape mode bound state, $P = 2\pi/\tilde{w}_s \approx 5.1302$. The black curve corresponds to the analytical second order approximation to $\hat{A}(t)$, namely equation (28) with $A(0) = \hat{A}(0) = 0.02$. Also shown is a zoom of the first oscillations of the amplitude of the internal mode; $A(t)$.

that the amplitude of the shape mode should decrease with time following the expression⁸

$$\frac{3}{4} \frac{d\hat{A}^2}{dt} = -0.0112909 \hat{A}^4, \quad (27)$$

which means that the amplitude should have the following time dependence:

$$\hat{A}(t)^{-2} = \hat{A}(0)^{-2} + 0.0150546 t. \quad (28)$$

Using the results in [32] we can also obtain the predicted form of the radiation field to be

$$f_r(x, t) = \frac{3\sqrt{3}\pi\hat{A}^2}{8\sinh(\pi\sqrt{2})} \cos \left[2\sqrt{\frac{3}{2}}t - 2x - \arctan(\sqrt{2}) \right]. \quad (29)$$

⁸ We give in the Appendix B a quick derivation of this expression following the calculations in [32] and adapting them to our current notation.

We have run different simulations starting with several values of the parameter $A(0)$ in order to check the accuracy of these theoretical expectations. In each case we extracted the value of the amplitude from the simulation by finding the perturbations around the kink and then projecting the perturbations over the shape mode (see Eq. (25)).

Our simulations demonstrate that the analytic predictions work perfectly in the case of a small initial amplitude for the bound state. In Fig 1 we show the comparison between the numerically time dependent amplitude $A(t)$ extracted using the expression given in Eq. (25) and the analytic prediction for $\hat{A}(t)$ (28). Remember that $A(t)$ carries information about the oscillatory part of the amplitude, whereas $\hat{A}(t)$ follows the envelope created by the maxima of the oscillations. Note that we have evolved this numerical computation for 2×10^5 times the period of the oscillation of the bound state.

We also show in Fig. 2 a snapshot of the perturbation field around the kink, as defined in Eq. (24). The central region can clearly be identified as the waveform of the shape mode (Eq. (9)), while the radiative small contribution far from the core is almost exactly a wave of twice the frequency of the shape mode in accordance with Eq. (29).

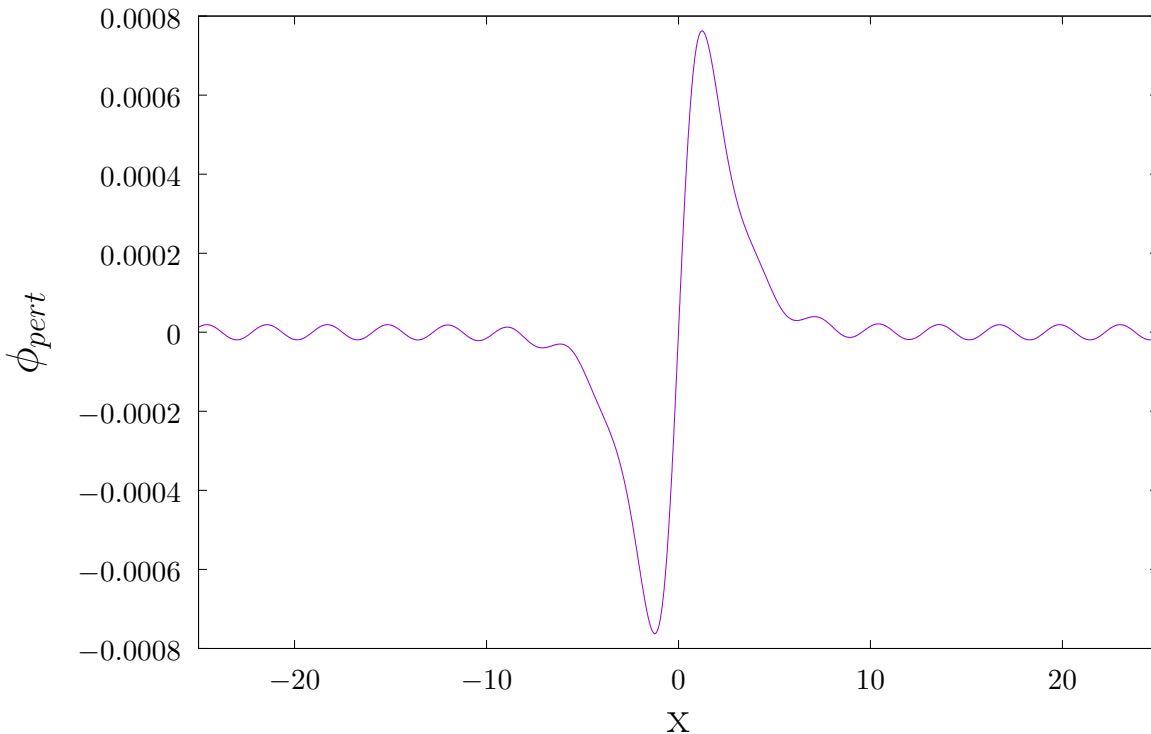


FIG. 2: Snapshot of the perturbation ϕ_{pert} around the kink.

We have also run simulations for larger values of the initial amplitude. The agreement with the analytic estimate is quite accurate all the way to $A(0) \sim O(1)$. This is somewhat surprising since the amount of energy stored in the perturbation in this case is above the kink rest mass, so there is no reason to expect this linear type behavior at this point. We show in Fig (3) the time evolution of the perturbation with $A(0) = 1$ as well as the analytic prediction for the envelope amplitude $\hat{A}(t)$.

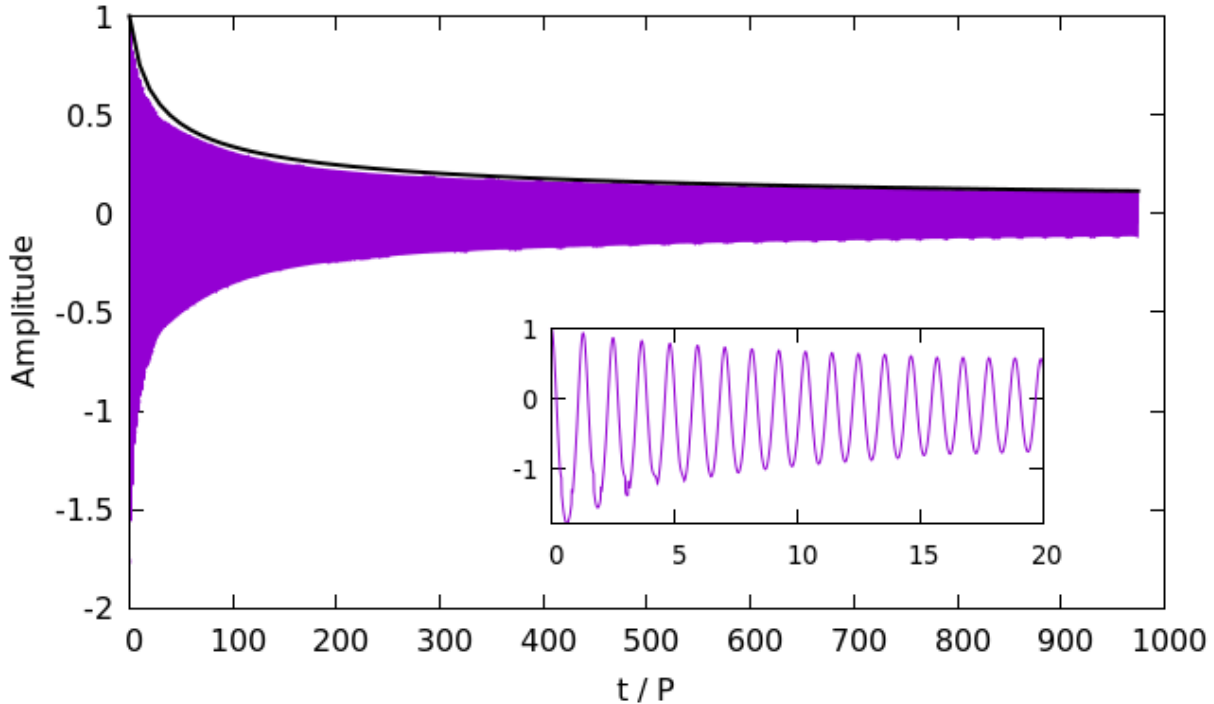


FIG. 3: Amplitude of the shape mode $A(t)$ as a function of time (displayed as number of periods or oscillations) for $A(0) = 1$. We show in the inset figure the first few oscillations of the amplitude where an initial asymmetric behaviour is clearly visible. This is a non-linear effect due to the initial large amplitude.

C. Non-linear evolution.

One can ask the question of what happens when one starts with a value of the amplitude well beyond the linear regime. As we mentioned earlier, going to such high values of the amplitude of the perturbation means that the energy of the configuration is not a small fraction of the energy of the kink solution. In fact, for high enough values of $A(0)$, the

energy of the initial state would be higher than the rest mass of the energy of 3 kinks. That means that there is enough energy to create a kink pair leaving behind an anti-kink at the center and still have a configuration consistent with the boundary conditions at infinity.

We have performed several simulations with those high initial energies and indeed we have found that for $A(0) > 1.334$ the final configuration is made of a central anti-kink with a couple of kinks flying away to infinity in opposite directions. This clearly indicates that one can think of the shape mode on a kink as a bound state of a kink-antikink-kink [32]. In fact, this is the way in which this type of mode was first discovered by numerical experiments in this model [33]. A collection of snapshots of the evolution of this process is given in Fig. 4.

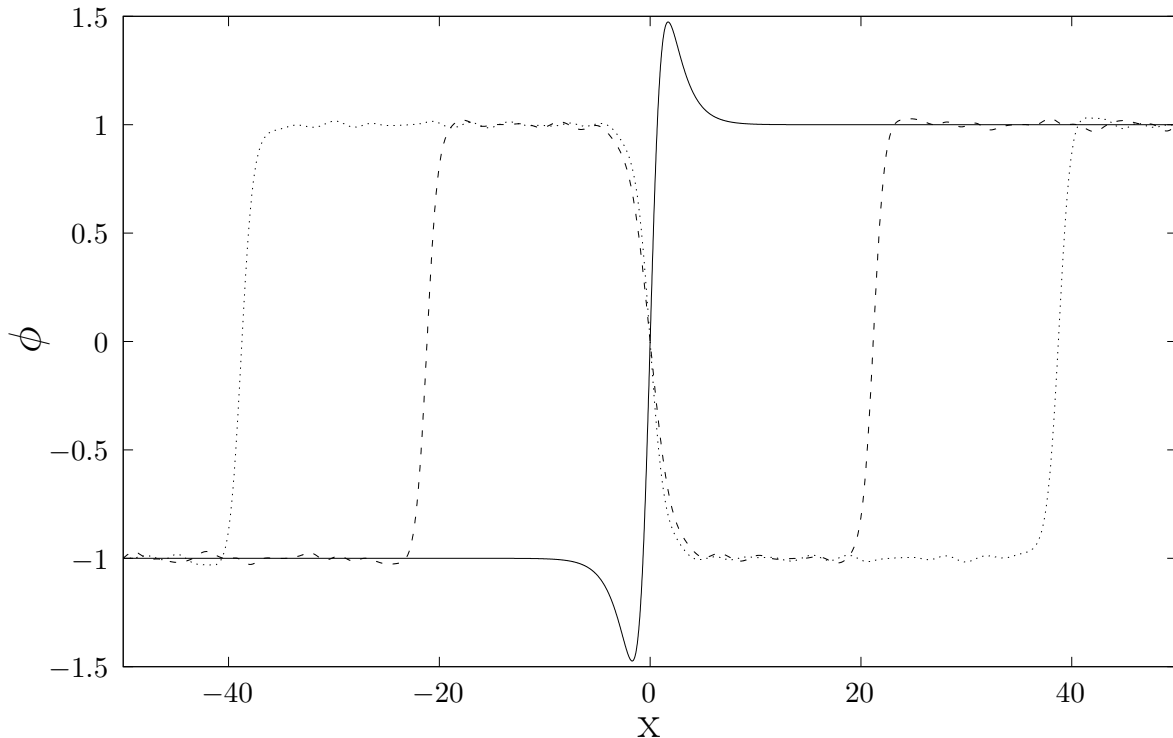


FIG. 4: Field profile at different time steps for $A(0) = 1.35$. A kink-antikink-kink system forms, and the kinks get away from the antikink in the middle. The solid line corresponds to the initial state, while the dashed and dotted lines correspond to the profile at $t = 80$ and $t = 160$ respectively (15.6 and 31.2 in units of the period of the shape mode P).

Going to higher energies than the threshold of kink-antikink formation produces a pair with higher initial velocities and leaves behind an anti-kink with some small amplitude of the shape mode still excited.

This non-linear process shows that there is a maximum amount of energy that can be stored in this long lasting bound state. Beyond that, the energy is shed by the soliton at a much faster rate in a time scale comparable to the light crossing time of the width of the soliton (one oscillation period). However, it is interesting to note that this maximum amount of energy could be even higher than the rest mass energy of the kink. This suggests that these modes could play a significant role in the dynamics of these solitons over the course of a long simulation. We shall therefore study next how these modes can get excited and to what extent this can happen in a realistic setting.

VI. NUMERICAL INVESTIGATIONS IN AN EXPANDING BACKGROUND

A. Preliminaries

Our main goal in this paper is to study the effects that excitations may have in the dynamics of the cosmological evolution of solitons. As a first step, we investigate a kink in a dynamic spacetime. Our starting point is therefore the same field theory as before but in a generic curved background with an action

$$S = \eta^2 \int d^2x \sqrt{-g} \left[\frac{1}{2} g^{\mu\nu} \partial_\mu \phi \partial_\nu \phi - \frac{1}{4} (\phi^2 - 1)^2 \right], \quad (30)$$

where g denotes the determinant of the $1 + 1$ metric in dimensionless units given by

$$ds^2 = dt^2 - a^2(t) dx^2. \quad (31)$$

We will take this spacetime as a fixed background; in other words, we will disregard any backreaction of the matter fields on this metric. Following this prescription we will specify the form of the function $a(t)$ and explore the dependence of the dynamics on its functional form in an attempt to simulate the different behaviour of the cosmological spacetimes one encounters in $3 + 1$ dimensions. Our conclusions must therefore be taken as an illustration of the possible effects on a full $3d$ evolution.

The equation of motion for the scalar field in this background becomes

$$\ddot{\phi} + H(t)\dot{\phi} - \frac{1}{a(t)^2}\phi'' + \phi(\phi^2 - 1) = 0, \quad (32)$$

where dots and primes denote derivatives with respect to cosmic time and comoving space

respectively, and $H(t) = \dot{a}(t)/a(t)$ is the Hubble rate⁹. In a slowly expanding spacetime, one can approximate the soliton by a solution of fixed physical width, namely a solution of the form

$$\phi(x, t) = \tanh \left[a(t) \frac{x}{\sqrt{2}} \right] . \quad (33)$$

This shows that for an expanding universe the width of the soliton shrinks in comoving coordinates. This is exactly the effect that we mentioned in the previous section. One should therefore be able to faithfully reproduce this evolution numerically if one is interested in studying excitations of the width of the soliton in an expanding universe.

In the following we will investigate the evolution of the kink solution in different spacetimes and with different initial conditions in order to see whether or not the evolution of spacetime and the environment can influence the presence of the shape mode.

B. The kink in an expanding universe

1. de Sitter space

One of the simplest expanding spacetimes that we can study and that will become useful in our future simulations is a 1 + 1 dimensional de Sitter space. In this case, the metric is given by

$$ds^2 = dt^2 - e^{2Ht} dx^2 . \quad (34)$$

The equation of motion for the scalar field in our dimensionless coordinate system becomes

$$\ddot{\phi} + H\dot{\phi} - \exp[-2Ht]\phi'' + \phi(\phi^2 - 1) = 0 . \quad (35)$$

Following the description above we can parametrize the solution of this equation as

$$\phi_{aS}(x, t) = \varphi_{aS}[Ha(t)x] , \quad (36)$$

so the function $\varphi(\xi)$ satisfies

$$(1 - \xi^2)\varphi''_{aS} - 2\xi\varphi'_{aS} = \frac{1}{H^2} (\varphi_{aS}^3 - \varphi_{aS}) , \quad (37)$$

⁹ Note that H is also written in dimensionless units and it is related to the usual dimensional Hubble rate by the relation $H_{\text{physical}} = \sqrt{\lambda\eta}H$

where now the primes denote derivatives with respect to the coordinate $\xi = Ha(t)x$.

This type of equation was originally found in [34] in the $(3 + 1)d$ context. The results here are parallel to the situation in higher dimensions since the longitudinal dimensions to the wall do not play a significant role. We can solve this equation numerically for different values of the Hubble parameter. For small values of H , the horizon distance is much larger than the width of the kink and therefore one expects the solution to be close to the adiabatic solution of a kink of constant physical width. In Fig. 5 we show the results for $H = 0.1$. We observed that in this case the deviation of the exact solution from the adiabatic one is very small. These deviations can be shown to scale with $O(H^2)$. Furthermore, similarly to what was found in [34], it can be seen that there is a maximum value of H beyond which there is no stationary kink solution. We will not explore this regime further in this paper.

We have checked that our numerical code on the lattice for a kink in a de Sitter universe reproduces the exact scaling solution given by Eq. (37). We have evolved the discrete equations of motion over several Hubble times without any visible excitation of the shape mode. See Fig 5 for a sample of solutions in comoving space.

Furthermore, in the regime where there is a separation of scales between the width of the soliton and the horizon size, we have also observed that an initial excitation of the internal mode on the kink lasts for long periods of time, following the same type of behaviour we have seen in Minkowski space background¹⁰.

In order to show this, we consider an initial configuration made up of a kink in de Sitter space, with $H = 0.1$, and we add a perturbation in the form of the shape mode with amplitude equal to $A(0) = 0.5$. This configuration is evolved for some time in de Sitter space and then we perform a smooth transition from de Sitter to Minkowski space so that the final scale factor has grown by a factor of ~ 30 .

There is a subtlety when performing these transitions between different spacetimes. These transitions change by definition the Hubble parameter and could themselves excite the internal mode of the kink solution. A fast transition from a de Sitter universe to flat space, for example, could trigger some excitation of the internal mode of the soliton. In order to have this effect under control, the final transition to Minkowski space has been designed to be a

¹⁰ Note that in this case, the bound state profile would be distorted as well, but in the regime we are interested in, it is sufficient to consider the same waveform as in flat space. This shape oscillates in the same way as before keeping the same physical width over time.

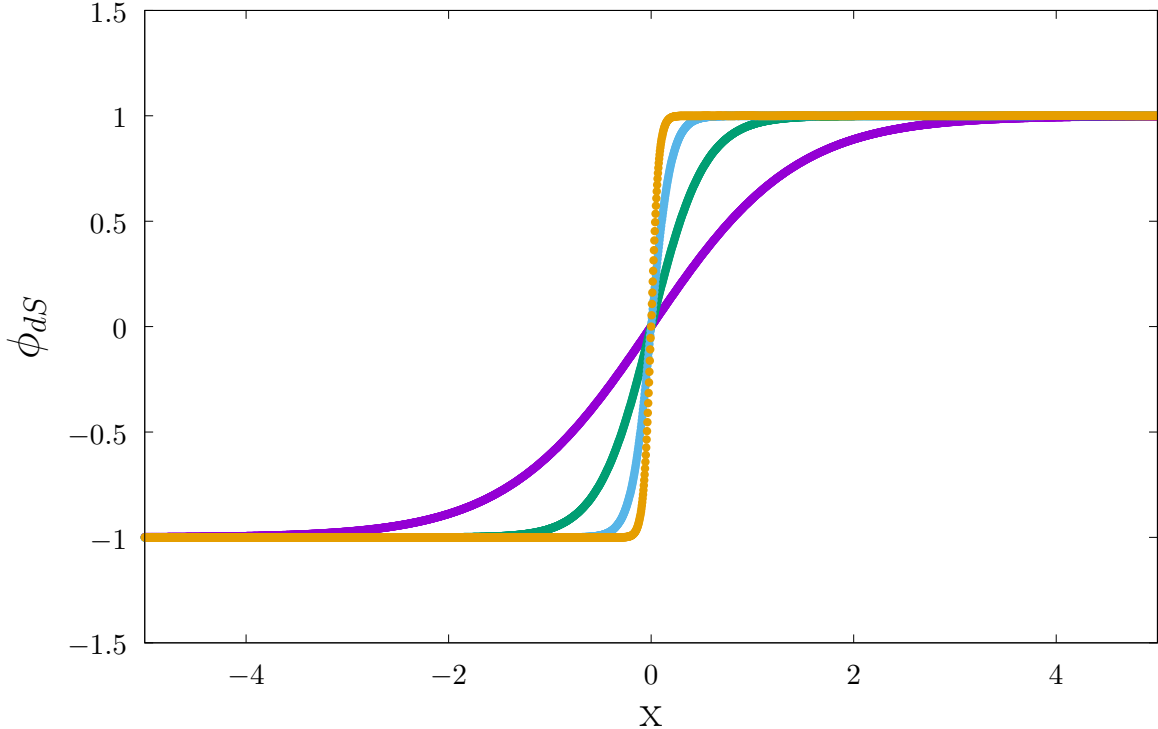


FIG. 5: Evolution of the kink solution in an expanding de Sitter space with $H = 0.1$. The different profiles correspond to expansion factors 1, $\exp(1)$, $\exp(2)$ and $\exp(2.96)$ (purple, green, blue and orange curves respectively). The solution matches perfectly the one obtained from Eq. (37).

smooth evolution on a time scale larger than the period of the oscillation of the bound state. We note that in this way the final result we read off from the simulation for the amplitude of the internal mode does not depend in any appreciable way on the details of the transition.

We obtain the amplitude of the shape mode by projecting out on the perturbation, as explained in Eq. (25)¹¹. As it can be seen in Fig 6, the amplitude of the shape mode stays quite constant during all this cosmological evolution.

These two numerical experiments allow us to conclude that evolving a kink in de Sitter spacetime of Hubble radius a few times larger than its size does not have much effect on the amplitude of the shape mode.

¹¹ In a dynamic spacetime we use the same type of projection assuming a fixed physical size of the soliton

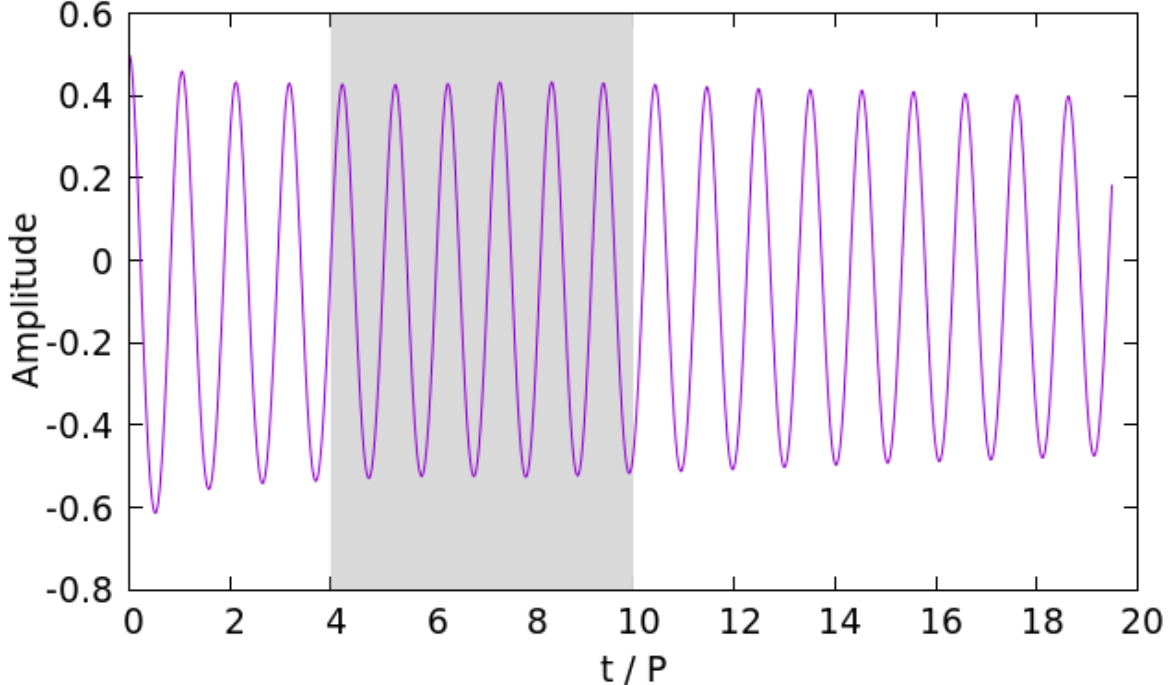


FIG. 6: Amplitude of the bound state $A(t)$ over several oscillations evolving in an expanding de Sitter background with a small expansion rate $H = 0.1$. We then transition from de Sitter space to Minkowski space in a smooth way (shaded region) to find that the amplitude stays pretty much constant. Time is given in units of the dimensionless oscillation period of the shape mode P .

2. Radiation dominated universe

We have also studied a power law behavior of the scale factor of the form $a(t) \sim t^{1/2}$. We call this "radiation dominated universe" for its close analogy with the $(3+1)d$ case. The important point about this type of dynamics is that the Hubble parameter changes over the course of the evolution in contrast to what happens in de Sitter space. We have not been able to find an exact expression for the kink profile in this spacetime. We can however approximate the solution by taking an *adiabatic* ansatz of the form

$$\phi_r(x, t) = \varphi_r[a(t)x], \quad (38)$$

which leads to the equation

$$(1 - H^2(t)y^2)\varphi_r'' = \varphi_r^3 - \varphi_r. \quad (39)$$

This equation can be used to find an approximate initial configuration for the kink in this

expanding universe by solving it at a particular value of time with $H = H_0$. This allows us to investigate the possible evolution of the bound state in this spacetime.

We performed the simulations using our parallel code (so as to ensure a fine enough grid to resolve the region of the kink in an expanding background). We also carefully change the background from radiation domination to Minkowski, so as to not excite the shape mode in the process (as explained earlier).

Our numerical results indicate that starting with a Hubble length somewhat larger than the width of the kink, the expansion of the universe does not affect significantly the amplitude of the bound state. This is in agreement with the results in de Sitter space and the intuition that a small expansion rate cannot have much influence on the dynamics of the internal mode, whose frequency is quite higher than H .

VII. PHASE TRANSITIONS IN AN EXPANDING BACKGROUND

We are now ready to investigate the main topic of this paper: the formation and perdurance of excitations on a kink in a cosmological setting where the soliton is embedded in a dynamical background. In this section, we will study numerically the formation of kinks in a phase transition and extract the level of excitation of the kinks in this process.

In order to simulate the phase transition, we will assume that the potential for the scalar field changes abruptly at some particular moment in time. In other words, we will consider a time dependent potential that evolves according to the following prescription ¹²

$$V(\phi) = \begin{cases} \frac{\lambda\eta^4}{4} + \frac{1}{2}m^2\phi^2 & \text{for } t < 0 \\ \frac{\lambda}{4}(\phi^2 - \eta^2)^2 & \text{for } t > 0 \end{cases} \quad (40)$$

where we will take $m^2 = 2\lambda\eta^2$ to be the mass of the field in the first stage of the evolution before the phase transition¹³.

Furthermore, we will consider the initial conditions of the field to be the ones of a thermal state of a massive free field at temperature T . There are other ways in which this thermal

¹² In this section we re-introduce dimensionful parameters briefly to clarify the physical content of the theory that we will simulate.

¹³ Note that this also corresponds to the mass of the perturbative excitations of the field around the vacua after the symmetry breaking transition.

state can be implemented, and we will discuss some of them in the following section. Here we will take an approach similar to the one used in [35], where the formation of oscillons was discussed. In our lattice field theory representation of the scalar field, this means that we will consider the initial state given by

$$\phi(x_j, t=0) = \sum_{n=-N/2+1}^{N/2} \frac{1}{\sqrt{2L\omega_n}} (\alpha_n e^{ik_n x_j} + \alpha_n^* e^{-ik_n x_j}), \quad (41)$$

$$\dot{\phi}(x_j, t=0) = \pi(x_j, t=0) = \sum_{n=-N/2+1}^{N/2} \frac{1}{i} \sqrt{\frac{\omega_n}{2L}} (\alpha_n e^{ik_n x_j} - \alpha_n^* e^{-ik_n x_j}), \quad (42)$$

where, as usual, we have discretized our box of size L on a lattice with spatial grid size Δx , so that the N sites of the lattice, x_n , are labeled by the index $n = -N/2 + 1 \dots N/2$. With this notation, the possible wave numbers of the reciprocal lattice are given by $k_n = 2\pi n/L$. Given the finite difference scheme described in Appendix A, one can see that the propagating free scalar field modes are parametrized by the frequencies

$$\omega_n = \sqrt{\left[\frac{2 \sin\left(\frac{k_n \Delta x}{2}\right)}{\Delta x} \right]^2 + m^2} . \quad (43)$$

Finally, the coefficients of the mode expansion α_n are given by a Gaussian Random Field whose two point function is given in terms of the thermal spectrum of the form

$$\langle |\alpha_n|^2 \rangle = \frac{1}{e^{\omega_n/T} - 1} = \frac{1}{2} \left[\coth\left(\frac{\omega_n}{2T}\right) - 1 \right] . \quad (44)$$

Rewriting this initial configuration in terms of our dimensionless coordinate system, the spectrum now reads

$$\langle |\tilde{\alpha}_n|^2 \rangle = \frac{1}{2\eta^2} \left[\coth\left(\frac{\tilde{\omega}_n}{2\eta^2\theta}\right) - 1 \right] , \quad (45)$$

where, as before, the quantities with tildes are dimensionless so $\tilde{\omega} = \omega/(\sqrt{\lambda}\eta)$ and the pre-factor η^2 is introduced to ensure that our expansion of the field is in agreement with our coordinates. This thermal state is therefore fully specified by two dimensionless parameters, namely,

$$\theta = \frac{T}{\sqrt{\lambda}\eta^3} \quad \text{and} \quad \eta . \quad (46)$$

The origin of the first one is clear since it controls the ratio of the typical thermal energy to the energy scale associated with the kink solution (see for example the expression of the

mass of the soliton in Eq. (3)). The appearance of η explicitly can be traced to the fact that our distribution takes into account the quantum effects of the Bose-Einstein distribution. Indeed, in the classical limit where $\omega_n \ll T$ the distribution becomes the Rayleigh-Jeans one and the explicit dependence on η disappears.

In the following simulations we will choose the parameters so that the amount of initial energy in the thermal state is subleading with respect to the potential energy of the vacuum state. Moreover, we will also take the quantum cutoff of the Bose-Einstein distribution at high frequencies such that this corresponds to a wavelength slightly larger than the lattice spacing. Both these facts will ensure that our initial conditions are dominated by a classical regime so that the use of classical equations of motion to obtain the distribution of defects in the transition is justified. We will fix θ and η so that both these requirements are satisfied in our simulations.

A. Evolving in an expanding background

The formation of domain wall solitons in a cosmological phase transition involves, of course, an expanding universe. In that regard it is interesting to perform our numerical simulation in this type of background. However, there is another reason to do this simulation in an expanding universe: it provides the simulation with a natural friction term. In fact, the background energy density present at the beginning of the simulation is very large compared to the average energy density expected as a final product of the transition in order to identify the individual kinks. This means that a mechanism for dissipation of this extra energy is needed. Without an efficient dissipation, kinks would acquire large kinetic energies and would annihilate with each other easily, leaving behind a large collection of perturbative excitations. Even if we manage to create a simulation with large enough volume where some of the kinks would survive for long time, the background energy would continuously excite the internal modes of the kink. In such case it would not be clear when to stop the simulation to obtain an accurate evaluation of the level of excitation of any internal modes present in the defects.

One can imagine fixing this problem by simulating the transition with some added friction term, but this is somewhat arbitrary since one would be able to control the final result by adjusting the amplitude and duration of the friction. This is why performing the simulations

of the transition in an expanding spacetime is advantageous. With the natural friction it provides, the background energy density slowly depletes. Furthermore, as we showed in our previous section, taking a small enough expansion rate does not affect much the amplitude of the internal mode of the kink solution.

This cosmological friction term also induces a horizon size, so kinks and anti-kinks present at distances larger than this distance are not to annihilate. Their velocities are redshifted until they are comoving with the background.

All these effects will allow us to obtain a much more realistic final configuration of the transition where kinks are well separated and almost at rest with respect to the simulation grid. This is a simple configuration that can be used to extract the amplitude of the internal mode of the kinks.

As a final step in the simulation, we also consider a smooth transition of the background to 1+1 dimensional flat Minkowski spacetime, as explained earlier. We evolve the simulation over large periods of time with absorbing boundary conditions, tracking the amplitude of the shape modes of the kinks.

B. Results

We have run several simulations of $N = 5000$ points with $\Delta x = 0.01$ with an initial thermal state that corresponds to a dimensionless temperature of $\theta = 10^{-3}$ and a value of the parameter $\eta = 250$. For these values of the parameters, the initial amount of thermal energy is of the order of 15% of the total background energy density. This also means that the thermal modes are substantially suppressed for wavelengths smaller than $\lambda_T \approx 10\Delta x$. So the thermal spectrum at the scale of the soliton is correctly represented by a classic thermal state.

We have evolved these initial configurations in an expanding de Sitter background whose Hubble constant in dimensionless units was set to $H_i = 0.04$. This means that the associated horizon size is substantially larger than the size of the kink soliton. Following the numerical experiments we described in the previous section, we are confident that any initial amplitude on the internal mode of the kink produced by the dynamics of the phase transition will survive in this background. Moreover, the background energy density of perturbative excitations is heavily suppressed during this time.

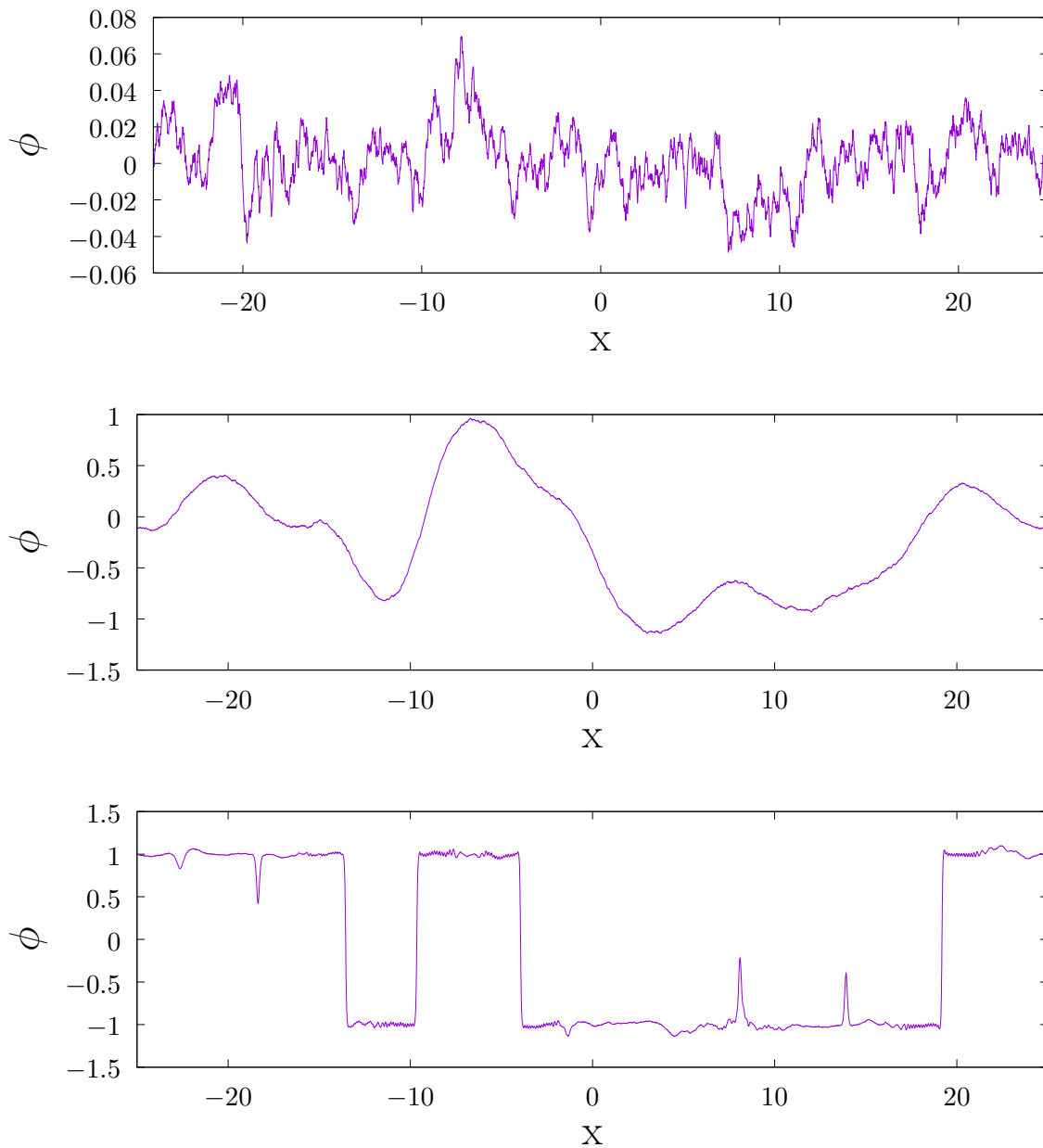


FIG. 7: Three snapshots of the field profile during the phase transition. The top one corresponds to the initial conditions. The middle one is at some intermediate step during the de Sitter phase and the bottom one is at cosmic time $t = 140$ (27.3 in units of the oscillation period of the shape mode P). This last instant of time already corresponds to the Minkowski stage. Several kinks and antikinks have been created.

We show in Fig. 7 a few snapshots of the field at different times for a particular realization of this setup. We notice that as time evolves the field settles on one of the vacua in different

regions of space. This leads to the formation of a "network" of alternating kinks and anti-kinks. Furthermore, this transition also leads to the generation of localized oscillating lumps around each of the vacua. These are nothing more than the breather type solutions that we discussed in previous sections. They are readily produced by the relaxation mechanism of the system directly and also by the collision and merging of nearby kinks and anti-kinks.

We let the system evolve until $t \approx 80$, where we relax the expansion of the universe smoothly into flat Minkowski space similarly to what we did in the previous section. By this time the background energy has already decreased substantially and one can observe the kinks forming. We also use absorbing boundary conditions so that radiation is allowed to be absorbed by the boundary and leave the simulation. The late time result of this simulation is a system of well separated kinks and anti-kinks, pretty much at rest with respect to one another, plus a collection of breathers.

We concentrate on each of the kinks and investigate their level of excitation by extracting the amplitude of the internal mode for each kink using the expression given by Eq. (25) locally. The results for the amplitudes of the kinks in one single realization are displayed in Fig. 8. We notice that the resulting amplitudes of the internal modes for the different kinks are quite similar.

In order to find the average value of this amplitude of the shape mode bound state, we have run 500 realizations with a thermal distribution of initial perturbations with $\theta = 10^{-3}$ to get that

$$\langle \hat{A} \rangle_{\text{formation}} = 0.5 \pm 0.1 . \quad (47)$$

We have also investigated the dependence of this quantity on the initial conditions by changing the temperature of the initial thermal state so that the percentage of extra initial energy due to this perturbations was smaller by a factor of 2. However, the final result for the average amplitude of the bound state of the kink was pretty insensitive to these changes. This may be attributed to the fact that the relevant energy scale in the process of the kink formation is the initial background energy associated with the initial vacuum state. In other words, the initial thermal fluctuations are important to induce inhomogeneities that lead to the formation of kinks and anti-kinks but not to the final energy stored in them.

We have also run simulations where the expanding spacetime was described by a "radiation domination" scale factor. The results are qualitatively similar to the case of de Sitter space.

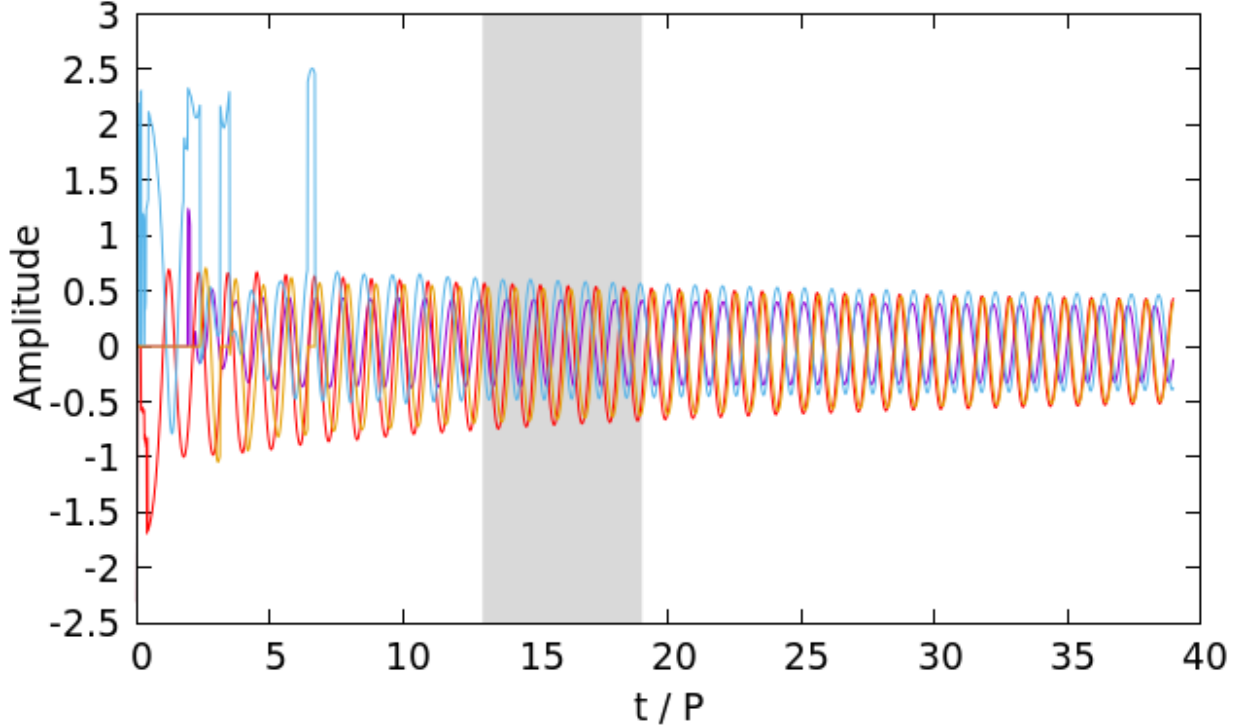


FIG. 8: Amplitude of the shape mode $A(t)$ as a function of time, for each of the four kinks in Fig. 7. The color correspondence is purple, red, blue and orange as we encounter the kinks going from left to right in Fig. 7. Time is given in units of the oscillation period of the shape mode P , and the shaded region represents the smooth transition from de Sitter to Minkowski space.

The movies produced from these simulations show that the excitation of the kinks is due to mainly two effects. The first one is the interaction of the kinks with the perturbative excitations on both sides of the soliton that pass through them. At a linear level, these modes should not excite the kink. However, at a non-linear level, these waves produce a non-zero excitation of the zero mode as well as the shape mode. We have actually tested this by recreating this type of interactions on isolated kinks that we irradiated with wave-packets of different frequencies. These scattering experiments indeed produced some motion of the kinks as well as an excitation of the internal mode.

The second mechanism for kink excitation is more non-linear in nature and has to do with the collision between breathers and kink-solitons. As we described in Section IV, one can consider the internal shape mode as a breather trapped on a kink. In fact, one can devise a low amplitude breather with very similar characteristics as the internal mode. Therefore, it should not come as a surprise that the collisions of breathers with kinks are a good place to

see the amplification of the energy stored in the internal mode.

We show in Fig. 9 three different snapshots of the field configurations for one such type of event. The initial configuration shows a kink and a breather at a short distance from one another. As times passes, the breather becomes closer to the kink and overlaps with it for a while. One can see that this triggers a big resonance effect on the amplitude of the internal mode, so the final state of the kink is substantially more energetic. See Fig. 10 for the evolution of the amplitude of the internal mode as a function of time ¹⁴.

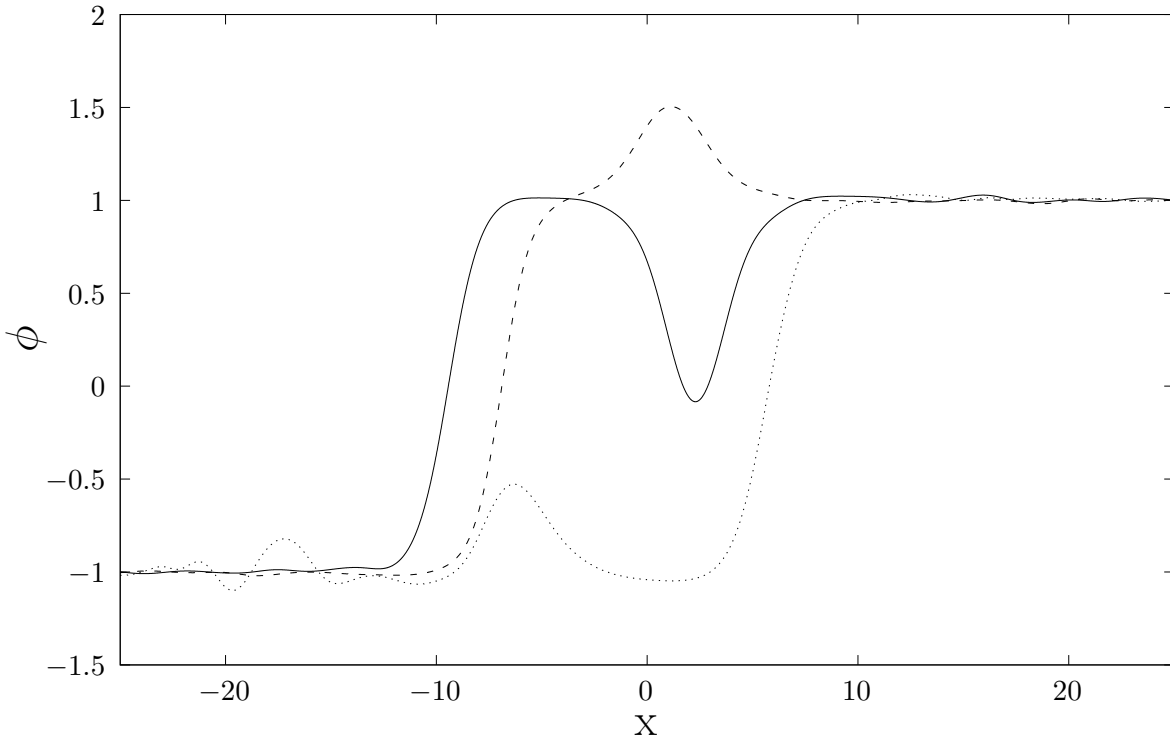


FIG. 9: Three different snapshots of the field showing the interaction between a kink and a breather. The solid line is the earlier configuration, the dashed line illustrates the two objects coming together, and the dotted line represents the result after they have passed through one another. The resulting amplitude of the shape mode in this scattering process is given in Fig. 10.

The combination of these two effects leads to the final amplitude of the shape mode on a typical phase transition. The kinks seem to have at formation around 20% more energy than the lowest energy configuration. This is not a negligible amount of energy, and it could easily have important consequences for the subsequent evolution. In particular, as we

¹⁴ The kink translational mode is also excited in this process.

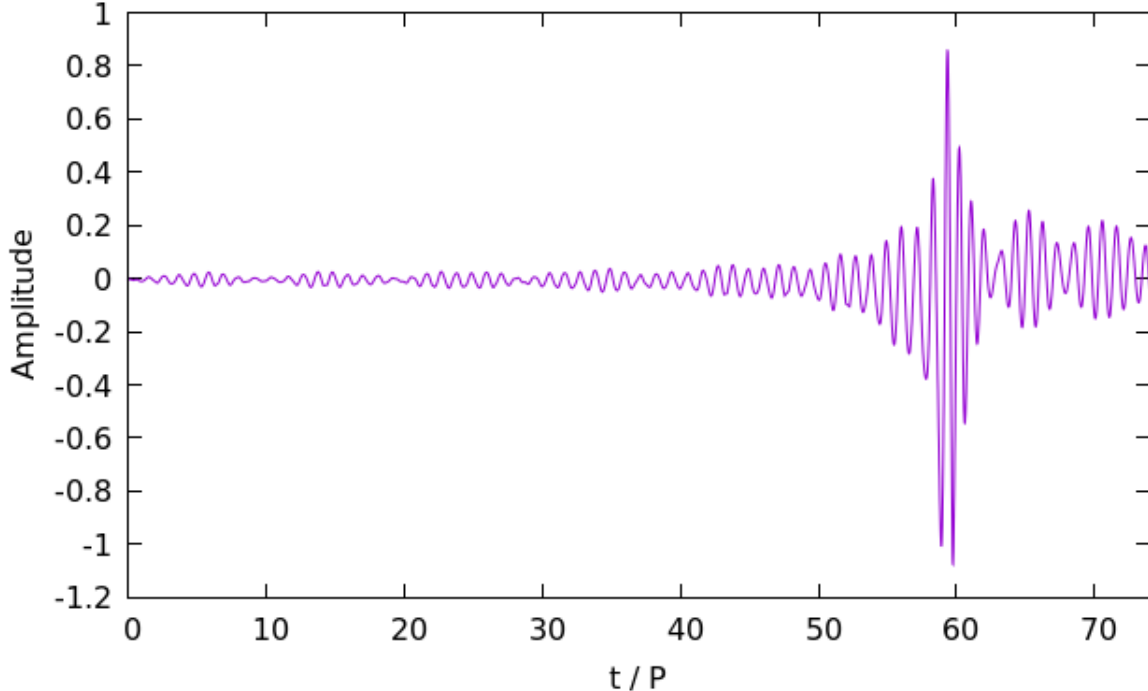


FIG. 10: Amplitude of the shape mode $A(t)$ as a function of time, during a collision of a kink with a breather. Time is given in units of the oscillation period of the shape mode P .

showed in Section VB, this kind of extra energy will stay in the kink for long periods of time compared to the natural time scale of the kink, which is given by $\tau \sim 1/m$.

VIII. HEATING UP THE KINK

Another interesting scenario is the possible excitation of the solitons due to their interaction with a thermal bath. This could happen, for example, in the formation of defects in a cosmological setting during reheating [36]. Alternatively, this could also be useful to estimate the possible degree of excitation in numerical simulations where there is a substantial amount of radiation in the background.¹⁵

There are several ways in which a thermal background can be simulated. Following the description in the previous section, we can approximate the solution of a kink in a thermal bath as a sum of the lowest energy configuration for the soliton together with a state of the

¹⁵ In this paper we have run the simulations with a thermal spectrum but could easily extend these ideas to include some other spectra.

form given by Eq. (41).

One could object that the presence of a kink will distort the spectrum of the perturbations around the solution, possibly affecting the amplitude of the bound state that we want to find. We have addressed this concern by simulating a thermal interaction of the kink with a bath using the Metropolis algorithm [37]. We give the details of this procedure in Appendix A 3. This is a much more expensive procedure computationally than the one described above, since the lattice needs to be swept many times over before a configuration that resembles the thermal state is reached¹⁶. We have done this for several different realizations and compared the results with the analytic setup of the thermal state described in the previous section to find that both these methods lead to comparable results for the amplitude of the shape mode.

We show in Fig. 11 a typical example of such initial configuration of a kink at a dimensionless temperature $\theta = 0.01$. Another important point to note is that the interaction with the thermal fluctuations imprints an initial velocity for the kink as well. We have checked that the distribution of initial velocities are in agreement with the expectation of a particle of mass M_k in a thermal state of temperature T . In practice, this initial velocity complicates the simulation in Minkowski space since for large temperatures the kink will eventually reach the boundary of our box and leave it.

We have therefore decided to simulate the initial thermal state in a de Sitter background with a small Hubble expansion rate. As we learned before, this does not have much of an effect on the amplitude of the shape mode, and it slows down the kink so that it can be simulated for large periods of time. This process allows us to reliably extract the value of the amplitude of the internal bound state. We have run 100 realizations for each temperature ranging from $10^{-4} < \theta < 2$ and obtained the average value of the amplitude of the kink. We have plotted the results in Fig. 12.

The analytic estimate of the average value of the amplitude as a function of the dimensionless temperature is described in Appendix C. This is done by looking at the projection of the thermal fluctuations over the bound state mode. This simple description implies that $\langle \hat{A} \rangle \propto \theta^{1/2}$. This is a good fit to our results at low temperature but deviates from the actual numerical results at higher values of the temperature. This is a somewhat expected result

¹⁶ This method has been previously used in the literature in similar models like [38].

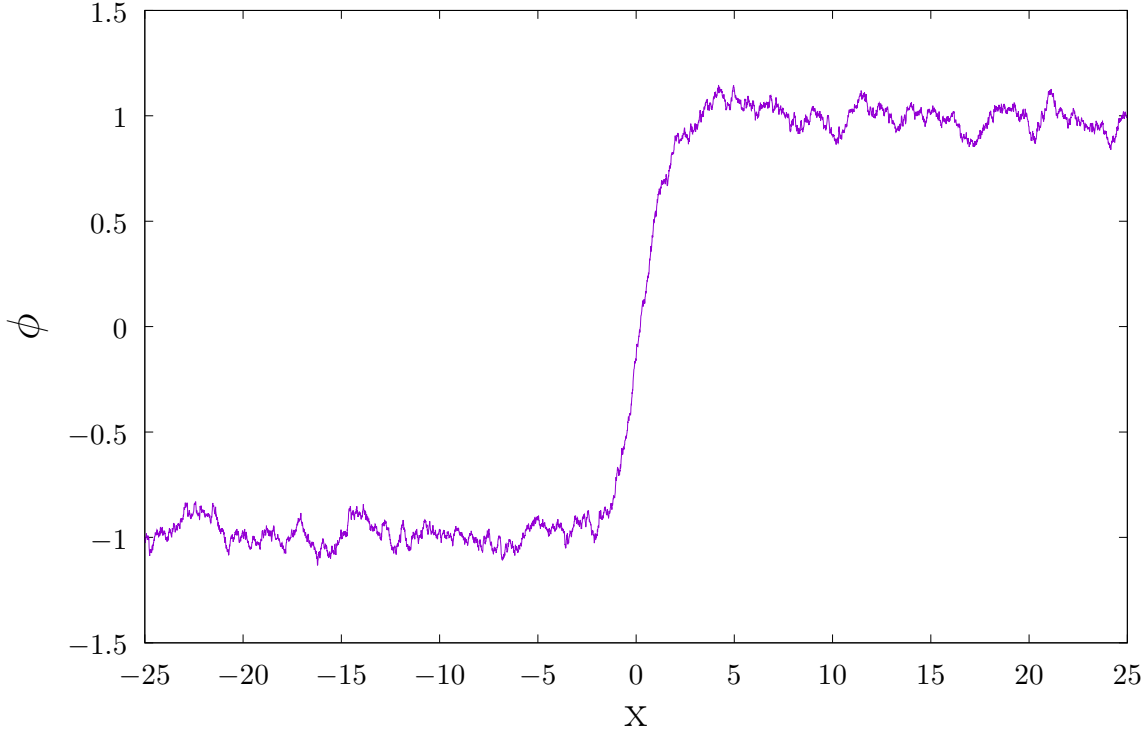


FIG. 11: Initial field configuration. It has been generated by means of the Metropolis algorithm, at temperature $\theta = 0.01$.

since the argument of the analytic estimate is based on purely linear approximation of the background radiation. However, as one approaches large temperatures, the amplitude of the thermal perturbations is not so small.

As we increase the temperature, we notice that the energy stored in the thermal fluctuations is not negligible compared to the energy of the kink. This means that in some realizations there are fluctuations that generate a kink-antikink pair directly from the background. For temperatures above $\theta = 0.2$, the number of these pairs is large.

We have performed these numerical simulations for temperatures as large as $\theta = 2$. In this case, the initial kink is irrelevant since the energy is so high that the typical fluctuations can go over the maximum of the potential. However, simulating this in an expanding background and with absorbing boundary conditions, we are able to end up with a collection of isolated kinks. We see that the amplitude of the kinks formed this way is of the order of $\langle \hat{A} \rangle \sim 0.5$. This is quite similar to the value we obtained in the previous simulations of the phase transitions.

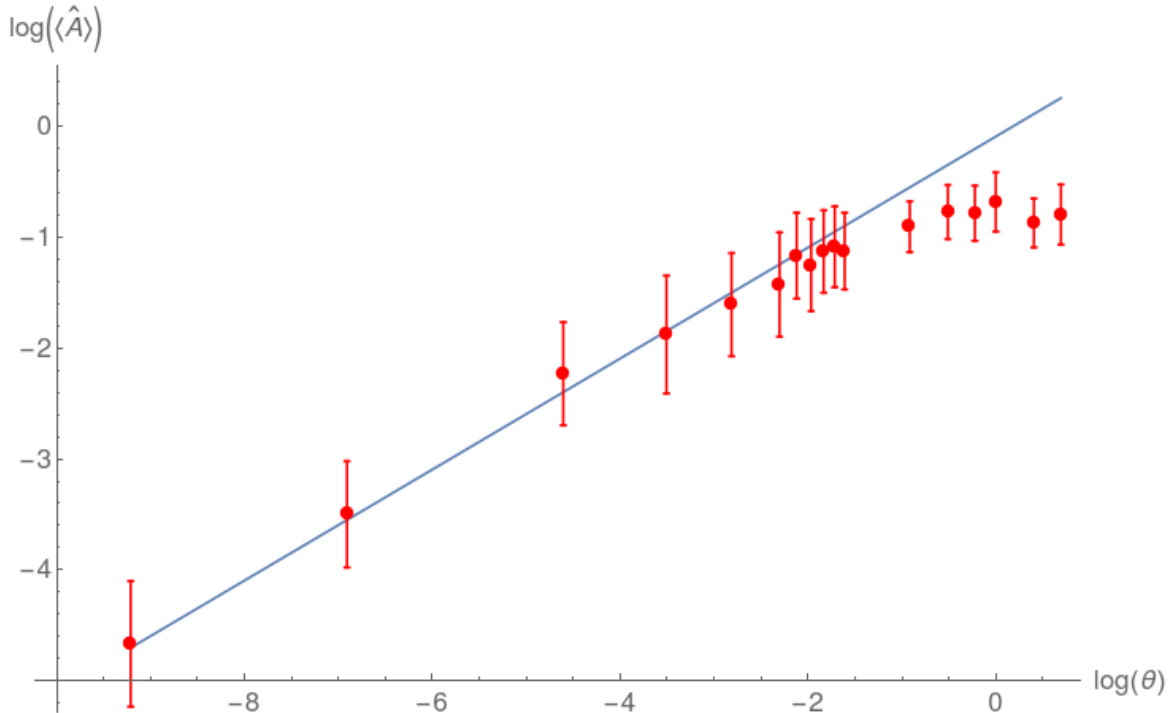


FIG. 12: Log-Log plot for the average amplitude of the shape mode $\langle \hat{A}(t) \rangle$, as a function of temperature. The amplitude is observed to tend to a constant value $\langle \hat{A} \rangle \approx 0.5$ in the high temperature limit.

It is interesting to note that one does not seem to be able to reach the strong non-linear regime for the shape mode amplitude in our numerical simulations. This is indeed the case for both models, the phase transition and the thermal bath interaction. One is tempted to speculate that even though the bound state could store much more energy, in practice, natural initial conditions for cosmology do not lead to such situations.

One can also simulate this interaction of the kink and a thermal bath using the Langevin equations (see for example [39]). It would be interesting to see if the results for the amplitude of the bound state in this case are in agreement with our simulations. We leave this question for future investigations.

IX. CONCLUSIONS

One of the most interesting properties of solitonic solutions for cosmological applications is their long lifetimes compared to the fundamental time scale of the underlying theory.

This is typically due to the fact that they correspond to the lowest energy configuration associated with a charge, either topological or non-topological, that ensures their stability.

In many field theory models, this long perdurance is also shared by other type of localized configurations that go by different names, such as breathers or oscillons. The reason for these other objects to have such a long lifetime is different. They are oscillating field configurations whose frequencies are below the frequencies of the propagating modes in the vacuum.

Here we study a sort of hybrid configuration, one that owes its long duration to dynamical reasons but lives on a soliton configuration. Perhaps the simplest example of this state is the localized excitation of the kink solution in $\lambda\phi^4$ theory. One can show that at a linear level there is such a bound state associated with the width of the kink solution and whose frequency is below the lowest frequency states in the vacuum. This means that, as in the case of oscillons, their decay is due to non-linear interactions.

In this paper we have studied the full non-linear evolution of such localized bound state of the kink soliton in Minkowski space. We have been able to do this over long periods of time by using a $(1+1)$ dimensional lattice field theory with absorbing boundary conditions. We have shown that one could store quite a large portion of extra energy on this bound state for times much longer than the natural time scale associated with their width. The similarities with the breather solutions in the theory makes us think of these bound states on the kink as a breather trapped in the core of the soliton.

We have also explored the evolution of these kink solutions in several cosmological backgrounds. In particular, we have run a large number of realizations to simulate a cosmological phase transition that leads to the formation of these defects. We found that the solitons will typically get formed with an approximately 20% of extra energy due to the presence of a substantial amplitude of the shape mode.

We have also simulated the interaction of the kink solution with a thermal bath and computed the average value of the expected amplitude of the bound state as a function of the temperature. As one increases the thermal energy of the background, the amplitude of the bound state grows following the relation $\langle \hat{A} \rangle \propto T^{1/2}$. This amplitude saturates when the extra energy of the soliton is also about 20%. This suggests that a purely thermal formation of solitons would also create them with some extra energy at this 20% bound.

Our results suggest that, in a realistic setting, solitons will always be formed in an excited state with some extra energy stored in their bound state modes. This could have

important consequences for the subsequent evolution of these objects. In particular, if this type of behaviour persists in higher dimensions, adding some extra energy to the solitonic configurations can easily affect their equation of state and hence their dynamics.

It is then clear that all these effects could modify the predictions of field theory simulations of these solitons since they could remain excited for the duration of the numerical span of the run. However, even though the lifetime of the bound states is very long compared to any time scale of the simulation, it is many orders of magnitude smaller than any relevant cosmological time. This means that one should also investigate whether there is any mechanism that maintains the level of excitation of the solitons throughout their cosmological evolution. Therefore, it remains to be seen if this initial energy that we report in this paper has a cosmological relevance or is just a short transient effect. We are currently investigating these ideas and we hope to report on them in the near future.

X. ACKNOWLEDGEMENTS

We are grateful to Ken Olum, Jose Queiruga, Tanmay Vachaspati, Manuel Valle and Alex Vilenkin for very useful suggestions and discussions. This work is supported in part by the Spanish Ministry MCIU/AEI/FEDER grant (PGC2018-094626-B-C21), the Basque Government grant (IT-979-16) and the Basque Foundation for Science (IKERBASQUE). The numerical work carried out in this paper has been possible thanks to the computing infrastructure of the ARINA cluster at the University of the Basque Country, (UPV/EHU), and the use of the Harria computer. We are grateful to Mariam Bouhmedi-Lopez for providing us access to Harria where some of this calculation were run.

-
- [1] A. R. Bishop, J. A. Krumhansl, and S. E. Trullinger, *Physica D Nonlinear Phenomena* **1**, 1 (1980).
 - [2] T. Skyrme, *Proc. Roy. Soc. Lond. A* **A260**, 127 (1961).
 - [3] J. Polchinski, *String theory*, Cambridge Monographs on Mathematical Physics (Cambridge University Press, 2007).
 - [4] A. Vilenkin and E. S. Shellard, *Cosmic Strings and Other Topological Defects* (Cambridge University Press, 2000), ISBN 978-0-521-65476-0.

- [5] Ya. B. Zeldovich, I. Yu. Kobzarev, and L. B. Okun, Zh. Eksp. Teor. Fiz. **67**, 3 (1974), [Sov. Phys. JETP40,1(1974)].
- [6] H. B. Nielsen and P. Olesen, Nucl. Phys. B **61**, 45 (1973).
- [7] G. 't Hooft, Nucl. Phys. B **79**, 276 (1974).
- [8] A. M. Polyakov, JETP Lett. **20**, 194 (1974).
- [9] A. E. Kudryavtsev, Pisma Zh. Eksp. Teor. Fiz. **22**, 178 (1975).
- [10] I. Bogolyubsky and V. Makhankov, JETP Lett. **24**, 12 (1976).
- [11] I. Bogolyubsky and V. Makhankov, Pisma Zh. Eksp. Teor. Fiz. **24**, 15 (1976).
- [12] M. Gleiser, Phys. Rev. D **49**, 2978 (1994), hep-ph/9308279.
- [13] K. D. Olum and J. J. Blanco-Pillado, Phys. Rev. D **60**, 023503 (1999), gr-qc/9812040.
- [14] K. D. Olum and J. J. Blanco-Pillado, Phys. Rev. Lett. **84**, 4288 (2000), astro-ph/9910354.
- [15] D. Matsunami, L. Pogosian, A. Saurabh, and T. Vachaspati, Phys. Rev. Lett. **122**, 201301 (2019), 1903.05102.
- [16] G. Vincent, N. D. Antunes, and M. Hindmarsh, Phys. Rev. Lett. **80**, 2277 (1998), hep-ph/9708427.
- [17] M. Hindmarsh, J. Lizarraga, J. Urrestilla, D. Daverio, and M. Kunz, Phys. Rev. D **96**, 023525 (2017), 1703.06696.
- [18] J. J. Blanco-Pillado, K. D. Olum, and X. Siemens, Phys. Lett. B **778**, 392 (2018), 1709.02434.
- [19] P. Auclair et al., JCAP **04**, 034 (2020), 1909.00819.
- [20] R. Rajaraman, *Solitons and Instantons. An introduction to solitons and instantons in Quantum Field Theory*, (North-Holland Publishing Company, 1982).
- [21] T. Vachaspati, *Kinks and domain walls: An introduction to classical and quantum solitons* (Cambridge University Press, 2010), ISBN 978-0-521-14191-8, 978-0-521-83605-0, 978-0-511-24290-8.
- [22] R. F. Dashen, B. Hasslacher, and A. Neveu, Phys. Rev. **D11**, 3424 (1975).
- [23] M. J. Ablowitz, M. D. Kruskal, and J. F. Ladik, SIAM J. Appl. Math. **36**, 428 (1978).
- [24] D. K. Campbell, J. F. Schonfeld, and C. A. Wingate, Physica D **9**, 1 (1983).
- [25] P. Anninos, S. Oliveira, and R. Matzner, Phys. Rev. D **44**, 1147 (1991).
- [26] H. Segur and M. D. Kruskal, Phys. Rev. Lett. **58**, 747 (1987).
- [27] P. M. Morse and H. Feshbach, *Methods of theoretical physics*, (McGraw-Hill Book Co., New York, 1953).

- [28] M. J. Rice, Phys. Rev. B **28**, 3587 (1983).
- [29] T. Romanczukiewicz and Y. Shnir (2018), 1809.04896.
- [30] W. H. Press, B. S. Ryden, and D. N. Spergel, Astrophys. J. **347**, 590 (1989).
- [31] B. Engquist and A. Majda, Mathematics of Computation **31**, 629 (1977).
- [32] N. Manton and H. Merabet, Nonlinearity **10**, 3 (1997), hep-th/9605038.
- [33] B. S. Getmanov, Pisma Zh. Eksp. Teor. Fiz. **24**, 323 (1976).
- [34] R. Basu and A. Vilenkin, Phys. Rev. D **50**, 7150 (1994), gr-qc/9402040.
- [35] E. Farhi, N. Graham, A. H. Guth, N. Iqbal, R. Rosales, and N. Stamatopoulos, Phys. Rev. D **77**, 085019 (2008), 0712.3034.
- [36] I. Tkachev, Phys. Lett. B **376**, 35 (1996), hep-th/9510146.
- [37] N. Metropolis, A. W. Rosenbluth, M. N. Rosenbluth, A. H. Teller, and E. Teller, The Journal of Chemical Physics **21**, 1087 (1953).
- [38] D. Y. Grigoriev and V. Rubakov, Nucl. Phys. B **299**, 67 (1988).
- [39] M. G. Alford, H. Feldman, and M. Gleiser, Phys. Rev. Lett. **68**, 1645 (1992).

Appendix A: Numerical details

1. Discrete Lattice evolution equations

We wish to solve numerically the following equations of motion (32):

$$\ddot{\phi} + H\dot{\phi} - \frac{1}{a^2}\phi'' + \lambda\phi(\phi^2 - \eta^2) = 0, \quad (\text{A1})$$

where dots and primes denote derivatives with respect to cosmic time and comoving space respectively, and $H = \dot{a}/a$ is the Hubble rate. For the numerical discretization of the equations of motion, first we revert to dimensionless quantities

$$\tilde{\phi} = \frac{\phi}{\eta} \quad \tilde{x} = \sqrt{\lambda}\eta x \quad \tilde{t} = \sqrt{\lambda}\eta t, \quad (\text{A2})$$

and dots and primes will now mean derivatives with respect to dimensionless quantities. The equation of motion now reads

$$\ddot{\tilde{\phi}} - \frac{1}{a^2}\tilde{\phi}'' + \tilde{\phi}(\tilde{\phi}^2 - 1) + \tilde{H}\dot{\tilde{\phi}} = 0, \quad (\text{A3})$$

where now $\tilde{H} = \frac{H}{\sqrt{\lambda\eta}}$ is the dimensionless Hubble rate. If the evolution takes place in Minkowski spacetime, it suffices to set $a = 1$ and $\tilde{H} = 0$. (From now on we will drop the tildes for simplicity)

We need to discretize equation (A3) into the lattice. In order to discretize the time derivatives, we use the so-called staggered leapfrog method. In order to do that, we need to define the conjugate momentum as

$$\pi\left(x, t + \frac{\Delta t}{2}\right) \equiv \frac{\phi(x, t + \Delta t) - \phi(x, t)}{\Delta t}. \quad (\text{A4})$$

Note that the field lives in integer time-steps, and the conjugate momentum in half time-steps. Now, the equation of motion for π reads

$$\dot{\pi} = \frac{1}{a^2}\phi'' - \phi(\phi^2 - 1) - H\pi. \quad (\text{A5})$$

First we discretize the second order spatial derivative of the field using nearest neighbours:

$$\phi''(x, t) = \frac{\phi(x + \Delta x, t) - 2\phi(x, t) + \phi(x - \Delta x, t)}{(\Delta x)^2}. \quad (\text{A6})$$

Since $\dot{\pi}$ will be evaluated at an integer time step as it is calculated as the difference of π at two different half-integer time steps:

$$\dot{\pi}(x, t + \Delta t) = \frac{\pi(x, t + \frac{3}{2}\Delta t) - \pi(x, t + \frac{\Delta t}{2})}{\Delta t}. \quad (\text{A7})$$

From (A5) we see that π and $\dot{\pi}$ should be evaluated at the same time step. However, the former lives at half-integer steps, while the latter lives at integer steps. To solve this issue, we simply replace π in the friction term with its average in neighbouring half time-steps:

$$\pi(x, t + \Delta t) = \frac{\pi(x, t + \frac{1}{2}\Delta t) + \pi(x, t + \frac{3}{2}\Delta t)}{2}. \quad (\text{A8})$$

Now all the terms in the equation for π (A5) are evaluated at integer time-steps. The staggered leapfrog method now consists of solving for the conjugate momentum using (A5), which explicitly reads

$$\begin{aligned} \pi(x, t + \frac{3}{2}\Delta t) = & \left(1 + H\frac{\Delta t}{2}\right)^{-1} \left\{ \left(1 - H\frac{\Delta t}{2}\right) \pi(x, t + \frac{1}{2}\Delta t) + \right. \\ & \left. + \Delta t \left[\frac{1}{a(t)^2} \phi''(x, t) - \phi(\phi^2 - 1) \right] \right\}, \end{aligned} \quad (\text{A9})$$

with ϕ'' given by eq. (A6), and then solving for the field, which can be obtained from eq. (A4):

$$\phi(x, t + \Delta t) = \phi(x, t) + \Delta t \pi \left(x, t + \frac{\Delta t}{2} \right). \quad (\text{A10})$$

The simulations are in 1-dimensional space, so in principle they are not very demanding, computer-wise. However, some of them have to be performed for very long periods of time. Moreover, since our simulation box is expanding in comoving coordinates, and the physical size of our objects is fixed, we encounter the problem that by the end of the simulation we may not have enough points to resolve out objects (the kink or the shape mode, e.g.) satisfactorily.

We thus wrote a parallel version of the code (also anticipating our higher dimensional simulations). The simulated (1-dimensional) box is distributed among different processors. Since our finite-difference scheme only relies on nearest neighbours, we only need a one dimensional halo around the box in each processor. We used *message passing interface* (MPI) for communication between different processors. A typical processor will share its information with the processors to either side of it. Except the first and last processors, which only share their information with one processor (to their right and left, respectively). On the other side of these processors, we apply the boundary conditions, absorbing boundary conditions, which are described below.

A typical simulation consists of a box of length $L = 50$, with $\Delta x = 0.01$ and $\Delta t = 0.0008$. Thus, the number of points in the box is $N = 5000$, which are distributed among 40 processors.

2. Absorbing Boundary Conditions

The idea behind these boundary conditions is quite simply to force an outgoing wave traveling towards the boundary to be annihilated at that point [31]. These conditions read

$$(\partial_x \phi + \partial_t \phi) \Big|_{x=\frac{L}{2}, t} = 0, \quad (\text{A11})$$

$$(\partial_x \phi - \partial_t \phi) \Big|_{x=-\frac{L}{2}, t} = 0. \quad (\text{A12})$$

At the boundaries, we will assume that the field can be written as a small perturbation around one of the vacua, namely, $\phi = \eta + \xi$. Let us consider a linear perturbation traveling,

for instance, towards the right boundary. The solution is given by

$$\xi(x, t) \propto e^{i(kx - \omega t)}. \quad (\text{A13})$$

The equation of motion for the perturbation, at $\mathcal{O}(\xi)$, is

$$\ddot{\xi} - \xi'' + m^2 \xi = 0. \quad (\text{A14})$$

The travelling wave (A13) is a solution to the equation of motion if $\omega^2 = k^2 + m^2$, but it only solves the absorbing boundary conditions if $\omega = k$. This means that these conditions will work perfectly for those modes with $k \gg m$, in other words, for the relativistic modes.

It is possible that the outgoing radiation in a particular problem is monochromatic, with known angular frequency ω . For instance, if our initial condition consists of a kink with its shape mode excited, we know that it will radiate waves with frequency $\omega = 2\omega_s = \sqrt{3}m$. In such a situation, the absorbing boundary conditions can be refined as follows:

$$\left(\frac{\omega}{\sqrt{\omega^2 - m^2}} \partial_x \phi + \partial_t \phi \right) \Big|_{x=\frac{L}{2}, t} = 0, \quad (\text{A15})$$

$$\left(\frac{\omega}{\sqrt{\omega^2 - m^2}} \partial_x \phi - \partial_t \phi \right) \Big|_{x=-\frac{L}{2}, t} = 0. \quad (\text{A16})$$

One can easily check that a traveling wave satisfying the equation of motion also satisfies these two equations. This means that for our almost monochromatic radiation this boundary conditions will be more effective. We have implemented these conditions and indeed the absorption gets to be better with this modified absorbing boundary conditions.

Here we show a couple of different situations to illustrate the way this absorbing boundary conditions work. We run our code twice in flat space with an initial condition given by an excited kink, but the excitations in both cases are quite different. In the first case, we use the bound state solution as the excitation with amplitude $A(0) = 0.332$. In the second case, we use a symmetric perturbation with the same amount of energy.

We plot in Fig. A2 the energy inside of our simulation box over the simulation time. We use the same boundary conditions in both cases. The results indicate several important points. First, the energy remains perfectly constant in both cases before any perturbation reaches the boundary. This means our code conserves energy in Minkowski space as it should. The energy curve in both cases starts to decline as soon as the first waves arrive to the boundary. However, the total energy from the symmetric perturbation decreases quite

rapidly and in a short period of time the final energy is the one of the kink itself. That means that the generic absorbing conditions work quite efficiently and there is not much energy bouncing around the box. In the other case, the energy curve decreases slowly due to the presence of the bound state that decays slowly. This slow leakage of energy is also efficiently absorbed in the boundary and the final result is also a small amount of feedback into the bound state due to energy bouncing off the edges of the box.

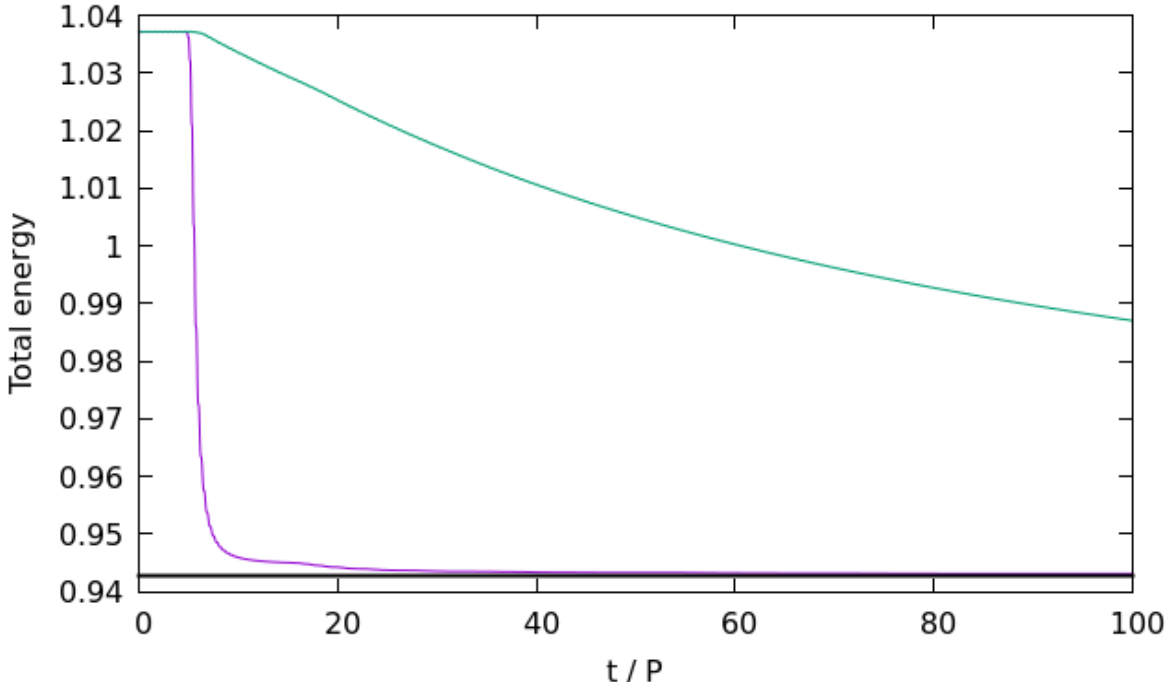


FIG. 13: Total energy inside of the box for two different initial conditions with absorbing boundary conditions. The green line shows the slow decay of the energy for a kink with a bound state excitation. The purple line represents the configuration of a kink with a symmetric perturbation. The total energy in this case is very quickly emitted from the kink and absorbed almost immediately as it reaches the boundaries.

3. Metropolis Algorithm for a thermal state

In the main part of the text we make use of a thermal state for a free massive scalar field as the initial conditions for some of our simulations. We do this by initializing the power spectrum of the field and its momentum so that their occupation numbers satisfy the Bose-Einstein distribution.

Here, we use an alternative way to arrive at this state that is based on the classic Metropolis algorithm [37]. This procedure is more flexible since it does not assume that we are in a free field vacuum. In fact, we will also use it to consider thermal fluctuations around the background kink solution, which may seem to be a more accurate method than the one used in the main text.

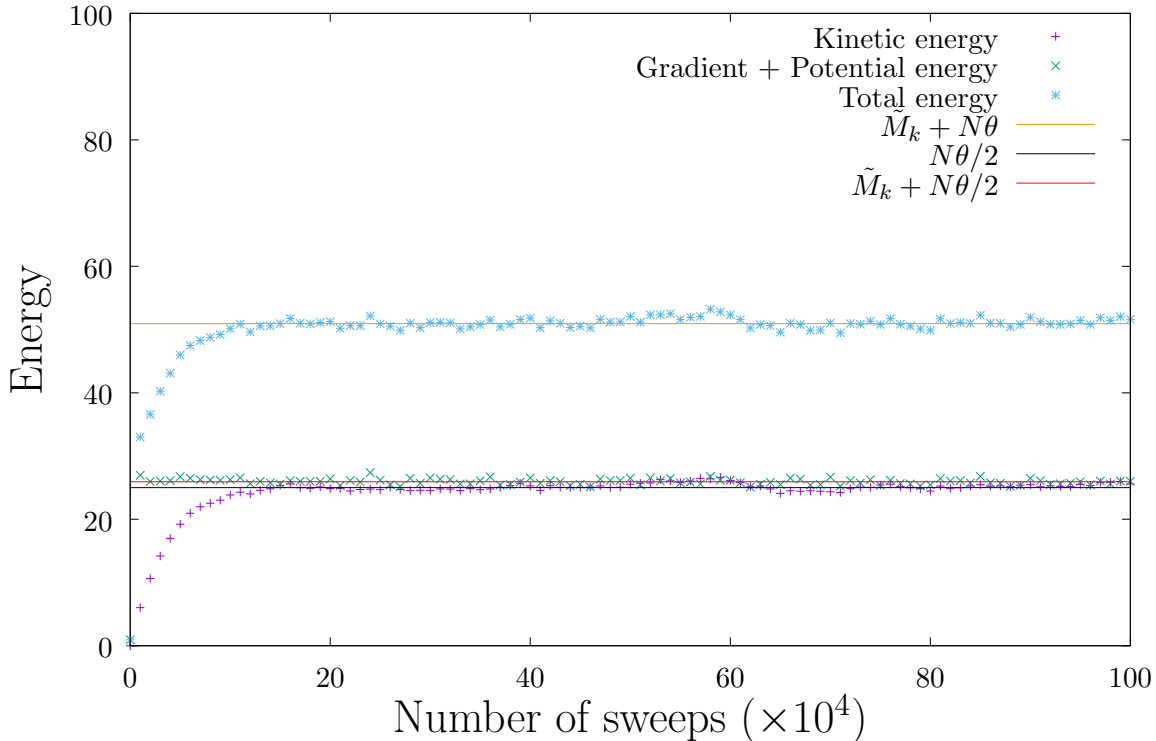


FIG. 14: Energy throughout the Metropolis algorithm (example with $\theta = 0.01$), taking the kink solution as initial state. The kinetic energy tends to $N\theta/2$, while the gradient+potential energy saturates to $\tilde{M}_k + N\theta/2$.

Let us briefly review the main steps to achieve this thermal state. The initial field profile for the algorithm is chosen to be a constant value at one of the vacua¹⁷ and we set the initial field velocity to zero. The algorithm then consists of the following steps:

1. We generate a new configuration which differs from the present one by changing the value of the field and its velocity at one lattice point¹⁸.

¹⁷ For the thermal state around the kink solution we start with the kink solution instead.

¹⁸ Since field and field velocity are independent variables, they must be varied independently.

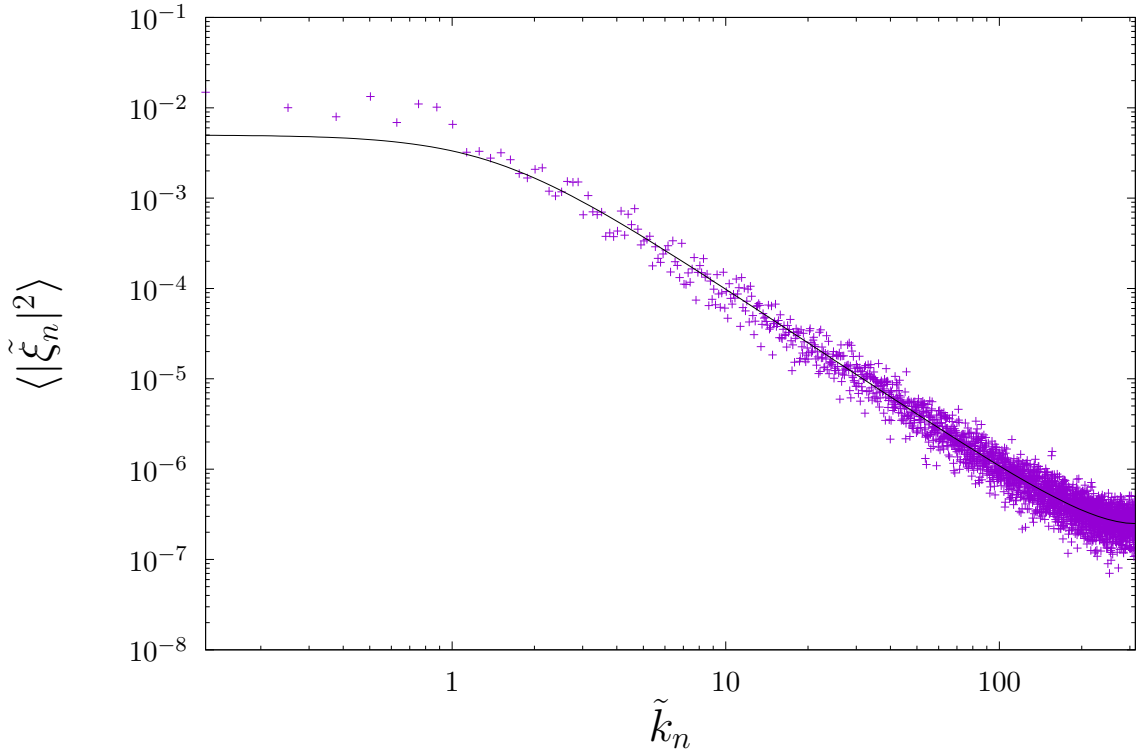


FIG. 15: Fourier spectrum of the thermal fluctuations $\tilde{\xi}$ at temperature $\theta = 0.01$ (average of 10 Metropolis realizations). The black curve corresponds to the classical limit of the theoretical spectrum at this temperature.

2. We then calculate the difference in energy between the new state and the old one:

$$\Delta\tilde{E} = \tilde{E}_{new} - \tilde{E}_{old}. \text{ Now there are two possibilities:}$$

- (a) The energy has decreased or remained the same: $\Delta\tilde{E} \leq 0$. In this case, we accept the change.
- (b) The energy has increased: $\Delta\tilde{E} > 0$. In this case, we accept the change with probability

$$p = e^{-\frac{\Delta\tilde{E}}{\theta}}, \quad (\text{A17})$$

with θ the temperature at which we are simulating. This can be done as follows. We choose a random number r between zero and one, $0 \leq r < 1$. If that number is less than the acceptance probability, $r < p$, then we accept the change. Otherwise, we leave the value of the field and the field velocity unchanged.

After that we just have to follow the same steps over and over again until the field reaches

thermal equilibrium. We will consider that the field is in a state of thermal equilibrium when the following two conditions are satisfied:

1. The total energy of the perturbations has saturated to $N\theta$, and it is equally stored in kinetic energy and gradient+potential energy, in agreement with equipartition (see figure 14).
2. The Fourier spectrum of both the field and the field velocity perturbations are well approximated by the classical limit of the theoretical thermal spectrum described in Eq. (45).

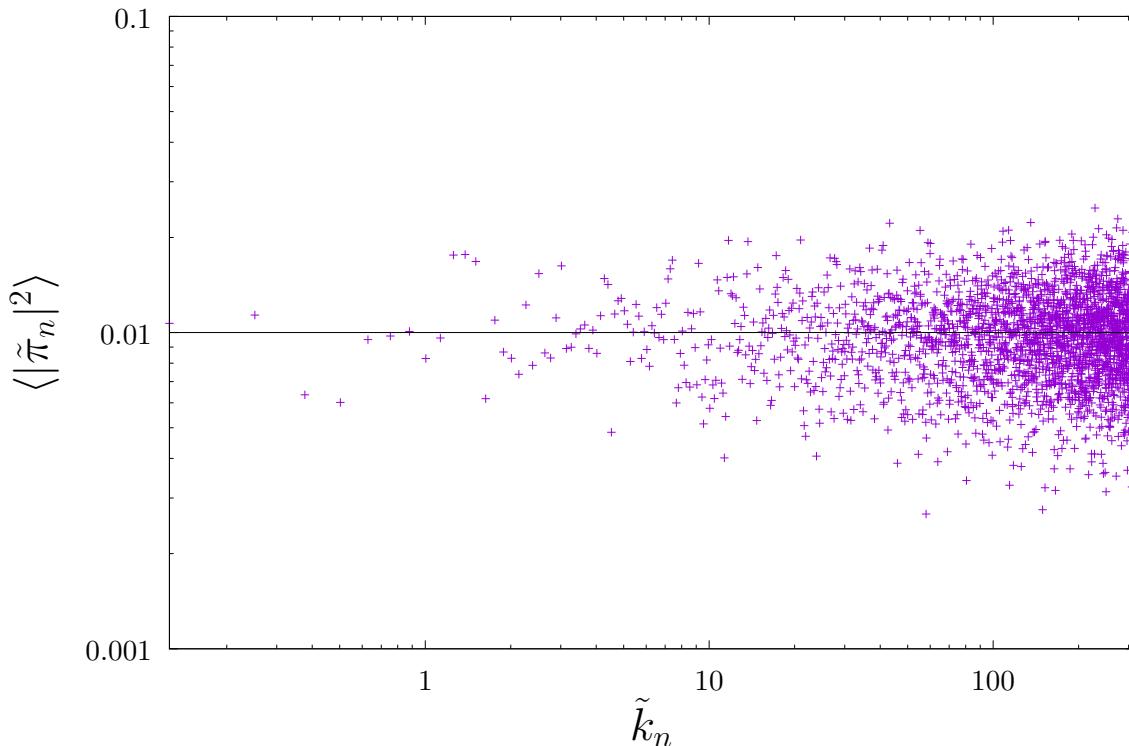


FIG. 16: Fourier spectrum of the velocity thermal fluctuations $\tilde{\pi}$ at temperature $\theta = 0.01$ (average of 10 Metropolis realizations). The black curve corresponds to the classical limit of the theoretical spectrum at this temperature.

We show in Figs. (15) and (16) the comparison of the different spectra obtained using the Metropolis algorithm and the classical limit of the theoretical spectrum at the same temperature. The coefficients $\tilde{\xi}_n$ are the Fourier coefficients of the thermal perturbation

field, and they are related to the $\tilde{\alpha}_n$ parameters used in the main text by

$$\tilde{\xi}_n = \frac{1}{\sqrt{2\tilde{\omega}_n}} (\tilde{\alpha}_n + \tilde{\alpha}_{-n}^*) . \quad (\text{A18})$$

The $\tilde{\pi}_n$ are the analogous coefficients for the field velocity:

$$\tilde{\pi}_n = i\sqrt{\frac{\tilde{\omega}_n}{2}} (-\tilde{\alpha}_n + \tilde{\alpha}_{-n}^*) . \quad (\text{A19})$$

We have also used the Metropolis algorithm to generate the spectrum of excitations of a kink in thermal equilibrium with a background. The simulations performed with these initial conditions yield statistically indistinguishable results from the classical limit of the spectrum Eq. (41). However, this method is much more costly in terms of time. This is why at the end we use the other method to generate a large set of realizations.

Appendix B: Analytical estimate of the decay rate of the bound state

As seen in the main text, at the linear level, the bound state (9) should oscillate with frequency $w_s = \sqrt{\frac{3}{2}}$ and should not decay, since its frequency is smaller than the frequencies of the propagating modes outside the kink. However, since the bound state couples nonlinearly to the propagating modes, the energy of the bound state is radiated away. As a consequence, the oscillating amplitude of the shape mode slowly decreases with time. The particular time dependence of the amplitude can be estimated analytically. Let us describe this estimation following the calculation given in [32], where we have adapted it to our notation.

We consider a parametrization of the field given by

$$\phi(x, t) = \phi_k(x) + A(t)\bar{f}_s(x) + f_r(x, t) , \quad (\text{B1})$$

where the $f_r(x, t)$ term is related to the propagating modes (10), and as said before, they are orthogonal to \bar{f}_s

$$\int dx \bar{f}_s(x) f_r(x, t) = 0 . \quad (\text{B2})$$

Plugging the decomposition in (B1) into the equation of motion, one can see that at the lowest order in A , the frequency of the oscillation is w_s , as we mentioned before. At the next order, at $O(A^2)$, the equation becomes,

$$\left(\ddot{A} + \frac{3}{2}A \right) \bar{f}_s + \ddot{f}_r - f_r'' + (3\phi_k^2 - 1) f_r = -3\phi_k \bar{f}_s^2 A^2 . \quad (\text{B3})$$

We can now multiply this equation by the shape mode function $\bar{f}_s(x)$ and integrate over all space, employing the orthogonality of eigenstates. This operation yields ¹⁹

$$\ddot{A} + \frac{3}{2}A = -3\alpha A^2, \quad (\text{B4})$$

where

$$\alpha = \int_{-\infty}^{\infty} dx \phi_k(x) \bar{f}_s^3(x) = \frac{3\sqrt{3}\pi}{32 \times 2^{3/4}}. \quad (\text{B5})$$

Substituting equation (B4) in (B3), one gets

$$\ddot{f}_r - f_r'' + (3\phi_k^2 - 1)f_r = 3(\alpha\bar{f}_s - \phi_k\bar{f}_s^2)A^2. \quad (\text{B6})$$

The expression of the amplitude can be written as (see eq. (23))

$$A(t) = \hat{A}(t) \cos\left(\sqrt{\frac{3}{2}}t\right), \quad (\text{B7})$$

where $\hat{A}(t)$ carries the information of the decay of the amplitude, and at linear order is a constant. The amplitude at $t = 0$ is $A(0) = \hat{A}(0)$.

This means that the source term on the right hand side of the Eq. (B6) has double that frequency. Manton et al. [32] were able to show that the solution of this equation for the asymptotic form of the radiation can be written as

$$f_r(x, t) = \frac{3\sqrt{3}\pi\hat{A}^2}{8\sinh(\pi\sqrt{2})} \cos\left[2\sqrt{\frac{3}{2}}t - 2x - \arctan(\sqrt{2})\right]. \quad (\text{B8})$$

Using this asymptotic solution for the field we can now find the energy flux radiated to infinity by the oscillating bound state. Including a factor of 2 to account for the radiation toward $x \rightarrow -\infty$ and averaging over a period, we get the radiated power to be

$$\frac{dE}{dt} = -0.0112909 \hat{A}^4. \quad (\text{B9})$$

Finally, the backreaction on the amplitude of the shape mode can be estimated on the grounds of energy conservation. It can be shown analytically that the energy of the field configuration

$$\phi(x, t) = \phi_k(x) + A(t)\bar{f}_s(x) \quad (\text{B10})$$

¹⁹ Note that according to the equation of linear perturbations, the term $-f_r'' + (3\phi_k^2 - 1)f_r$ is proportional to f_r , and therefore it is orthogonal to the shape mode.

is given by

$$E(t) \approx M_k + \frac{3}{4} \hat{A}^2(t) + \dots \quad (\text{B11})$$

provided that the amplitude is small.

Therefore, using energy conservation we obtain

$$\frac{3}{4} \frac{d\hat{A}^2}{dt} = -0.0112909 \hat{A}^4, \quad (\text{B12})$$

which yields

$$\hat{A}(t)^{-2} = A(0)^{-2} + 0.0150546 t. \quad (\text{B13})$$

This is the final result for the long term evolution of the envelope amplitude of the bound state in Minkowski space. In the main part of the text we will compare this with our numerical solutions.

Appendix C: Analytical estimate of the amplitude of the bound state at finite temperature

In section VIII we have seen that, at low temperatures, the amplitude of the bound state in a kink in thermal equilibrium follows a simple relation given by

$$\langle \hat{A} \rangle \propto \theta^{1/2}, \quad (\text{C1})$$

where $\langle \hat{A} \rangle$ is the average on an ensemble of realizations at temperature θ .

Here we give a simple derivation of this fact by first computing the probability density for the amplitude of the bound state at finite temperature and obtain from that the average amplitude. In order to do that, we will make the assumption that one can directly read the amplitude of the bound state by projecting the generic thermal state of the perturbation on the bound state mode waveform. This is possible due to the orthogonality relation of the different perturbation modes we found for the kink (see the discussion in Sec. V). It is important to note that this neglects the possible non-linear interaction between the different perturbations modes and the kink itself. This will limit the validity of our approximation to small amplitude perturbations or small temperatures.

As we described in Sec. VII, our initial configuration for a thermal state is given by a Gaussian Random Field with a thermal spectrum given by Eq. (44), which in the classical

limit becomes,

$$\langle |\alpha_n|^2 \rangle \approx \frac{T}{\omega_n}. \quad (\text{C2})$$

We can now project this configuration over the bound state by following the general prescription given by Eq. (25). Notice that in our discrete lattice this is nothing more than a linear combination of the coefficients for $\phi(x, t = 0)$. Similarly, one can find the initial velocity of the state by the analogous projection in the velocity field. Doing this exercise, we note that the distribution of the amplitude and the velocity must be given by another Gaussian Random Field with different values of their variance.

In our numerical experiments we characterized the amplitude of the bound state by its maximum value in the course of one oscillation, what we have denoted by the envelope amplitude \hat{A} . This means that in order to make a meaningful comparison with the calculation of the instantaneous projection we need to integrate over the possible phases that we happen to get in the initial conditions.

Following a somewhat lengthy but straightforward calculation one arrives to the probability density for the amplitude of the bound state obtained with this procedure to be

$$\rho(\hat{A}) = \mathcal{N}(\theta) \hat{A} \exp\left(-\frac{\hat{A}^2}{\sigma^2 \theta}\right) I_0\left(\frac{\hat{A}^2}{D^2 \theta}\right) \quad (\text{C3})$$

where I_0 is the modified Bessel function of the first kind and the coefficients σ , D and \mathcal{N} can be computed in terms of the parameters of the model and the proper normalization for the probability density.

Finally, taking this probability density into account, one can obtain that

$$\langle \hat{A} \rangle \propto \theta^{1/2}, \quad (\text{C4})$$

which is in pretty good agreement with the dependence found in Fig. 12. Note that at temperatures larger than $\theta \sim 0.5$ the numerical results start to deviate from the present analytical estimate. We attribute this discrepancy mainly to the fact that at those energies we are outside the linear regime.

Finally, we have tested these results numerically as well by computing the distribution of the observed values of the amplitudes of the bound state for 300 realizations of the initial conditions at a temperature of $\theta = 10^{-4}$. We show a reasonably good agreement in Fig. 17 by showing the amplitude distribution of these realizations and its comparison with the analytic curve given by Eq. (C3).

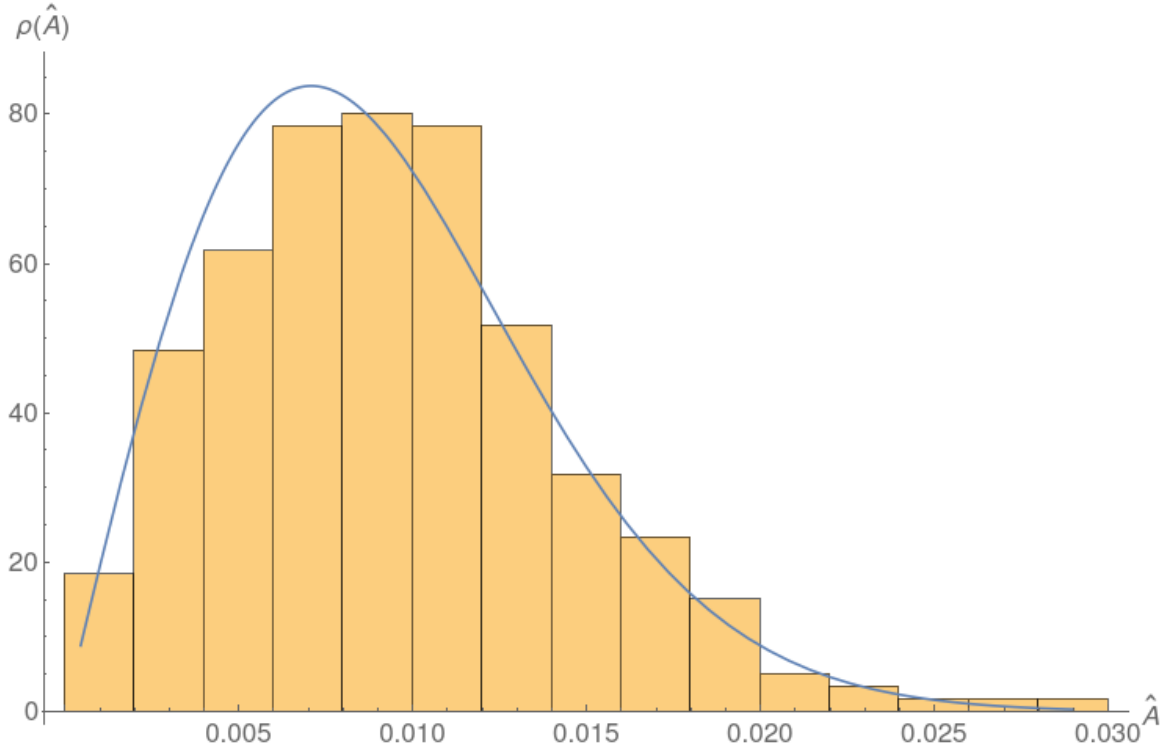


FIG. 17: Histogram of the probability density for the values of the amplitude of the bound state \hat{A} at a temperature $\theta = 10^{-4}$ from 300 simulations. The solid line represents the estimate of this distribution computed in Eq. (C3).